Ab initio Study of Tantalum Nitride and Silver Adatoms

by

Michael Grumski

A Dissertation Presented in Partial Fulfillment
of the Requirements for the Degree
Doctor of Philosophy

Approved April 2012 by the
Graduate Supervisory Committee:

James Adams, Chair
Stephen Krause
Terry Alford

ARIZONA STATE UNIVERSITY

May 2012

ABSTRACT

In 2022, integrated circuit interconnects will approach 10 nm and the diffusion barrier layers needed to ensure long lasting devices will be at 1 nm. This dimension means the interconnect will be dominated by the interface and it has been shown the interface is currently eroding device performance. The standard interconnect system has three layers – a Copper metal core, a Tantalum Adhesion layer and a Tantalum Nitride Diffusion Barrier Layer.

An alternate interconnect schema is a Tantalum Nitride barrier layer and Silver as a metal. The adhesion layer is removed from the system along with changing to an alternate, low resistivity metal. First principles are used to assess the interface of the Silver and Tantalum Nitride. Several stoichiometric 1:1 Tantalum Nitride polymorphs are assessed and it is found that the Fe_2P crystal structure is actually the most stable crystal structure which is at odds with the published phase diagram for ambient crystal structure. The surface stability of Fe_2P-TaN is assessed and the absorption enthalpy of Silver adatoms is calculated. Finally, the thermodynamic stability of the TaN-Ag interconnect system is assessed.

DEDICATION

The little fur ball who often gave me more trouble than any human could, but still makes me smile. She was always and still is beside me.

The man who will always be an example of who I am and what I should strive to be.

Thank you Elmer (Grandpap) Wolf and Pepper Grumski, you both are in my heart forever.

Pepper Grumski – 2000 to 2010

Elmer Wolf – 1918 to 2012

ACKNOWLEDGMENTS

I would like to thank all of those who have been at my side over the years, pressing and pushing me forward.

To my Intel Peers, Scott Buck, Subra Iyer, Matt Knowles, Kevin Heidrich and Bruce Gilmore, for their patience. To James Clarke, Adam Schafer, Ron Woodbeck and Rick Livengood who always provide support on how to improve and drive myself both intellectually and personally.

To my academic peers, Pratik Dholabhai and Shahriar Anwar, thank you for all of your guidance on ab initio Studies and on how to engage in an academic environment. Dr Amery and Dr Widenhouse as examples of what I can strive to be in industry.

To my committee, Dr Krause who always provided good guidance on both my early work and how to approach my current dissertation. To Dr Alford for his direct and generous feedback. To Dr James Adams for his constant sanity and intellectually insights on what the actual information means.

To my parents who always supported me through my education. To my Sister, In-laws and extended family who provide me with connections to what I should be on a regular basis.

To my pups', Liberty and Bella, who often remind me of the important aspects of life like; dessert and sleep. To my sons', Joshua and David, who often give me an opportunity to see what I really am and provide me incentive to improve. And finally to my intellectual peer and love, my wife, Bonnie, who often points out she did way, way better than I in the State Science fair prior to us meeting in college.

TABLE OF CONTENTS

Page

CHAPTER Page

LIST OF TABLES

LIST OF FIGURES

Figure Page

Chapter 1

INTRODUCTION

The semiconductor industry has been following Moore's law for approximately 50 years. The law is based on the economic scaling of the integrated circuits used in products from cell phones to laptops to supercomputers. The law basically predicts the doubling of the density of transistors in a device every two years or so. The continued compaction of devices and increased densities has allowed the growth and expansion of computational and technological innovations we are seeing over the course of the past 50 years. The continued pace of the semiconductor industry is reliant upon understanding how materials behave on atomic scales as the devices are approaching atomic dimensions.

In the 2020 timeframe, the interconnects will approach sub-10 nm's in width and the barrier/adhesion layers necessary for the metal lines to be produced will be < 2 nm in thickness. At these aggressive thicknesses, the interface of the metal line and the adhesion/barrier layer will become a critical barrier to further improvement in IC speed performance as the interface will be a primary contributor to the devices switching time. The time delay induced by the interface is due to electron scatter.

Currently, interconnects are layered structures of 3 materials with copper for the metal, tantalum for the adhesion layer and tantalum nitride for the barrier layer. Research is underway to assess alternate barrier/adhesion layer materials, but there are limited studies on alternate metals with barrier/adhesion layers. Silver has been suggested in the literature as an alternate metal to copper due to its improved bulk resistivity properties. This dissertation will attempt to assess an alternate path to allow for continued scaling of the interconnect by simplifying the material makeup. The work will be based on ab initio studies to help understand if there is a better material set for the interconnect.

The dissertation is organized as follows: The First Chapter discusses the Interconnect system and projected issues facing the metal wiring as it is scaled to continue the pace of Moore's Law. The Second Chapter reviews the materials typically used along with an overview of the selected alternate materials will be presented. The Third Chapter is a review of the ab initio technique employed in the studies. The remaining chapters are dedicated to the studies performed and the results of the dissertation.

This chapter is organized to highlight key technical underpinnings for the interconnect, issues with scaling of the system and proposes an alternate way of looking at the system. First an overview of the Interconnects is provided along with the key issues faced with the systems.

Interconnects

Modern Integrated Circuits (IC) have features on the order of 32 nm.[2] Figure 1 shows a cross section of an IC and the interconnects have around 10 levels. The levels include metal wiring in the plane of the wafer and metal VIA's which connect between layers. With continued scaling, IC interconnects will begin to approach 10 nm in width by 2020. The interconnects need low resistivity with copper being the most widely used metal. The move to Copper was induced by the fact that the first interconnect metal, Aluminum, had high resistivity and long term stability issue, namely electromigration.

Copper has issues with its use as it readily reacts with ILD and shorts devices. A barrier layer is used. The barrier is needed for copper and other highly conductive metals including silver or gold. State of the art metallization schemas use dual damascene processing where the interlayer dielectric (ILD) is patterned for 2 layers and

then a barrier layer is deposited followed by an adhesion layer with the metal deposited in a multiple step process.

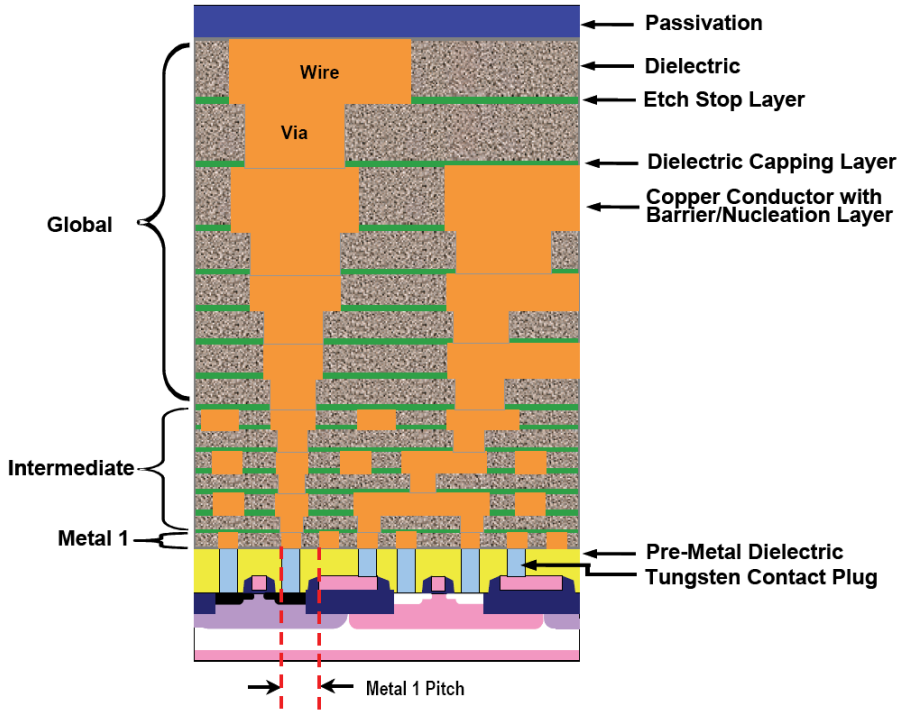

Figure 1. Cross Section of Integrated Circuit [2]

The adhesion layers are in place to enhance coating of the metal to the barrier layers. This results in a multi-layer, heterogeneous system that has 4 interfaces as shown in Figure 2. The complexity of the processing schema adds cost and potential yield issues due to integration complexity. In 2022, the barrier layer approaches atomic thicknesses with dimensions for the interconnect system provided in Table 1 along with typical materials used for the layer. [2]

The barrier and adhesion materials can change or be changed stoichiometrically, crystallographically, or chemically depending on the processing characteristics of the individual integrated circuit manufacturer. The common materials for barrier layers are refractory metals, nitrides and oxides as these show good resistance to copper diffusivity.

The barrier materials typically are not conducive to conformal coating by the interconnect metal. These composite systems are starting to have issues as they are approaching atomic dimensions.

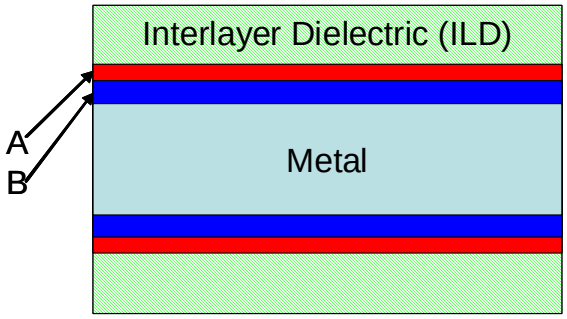

Figure 2. Cross Section showing all materials of an Interconnect. Layer A (red) is the Barrier Layer, Layer B (dark blue) is the Adhesion Layer.

Table 1. Modern Interconnect dimensions [2]

Layer	Width (nm) in 2022	Common Production Material
Metal Line	8 to 12	Copper
Adhesion Layer	0.8	Tantalum
Barrier Layer	0.8 to 1	tantalum nitride or titanium nitride
Interlayer Dielectric (ILD)	NA	carbon doped silicon dioxide

Interconnect Scaling Issues: Resistivity and Electromigration

The issues seen with Aluminum which prompted the move to the Copper Interconnect system are once again showing up as the dimensions of the device approaches atomic scale. The interface of the copper Interconnect system is central to the constraints of scaling the interconnects. The two issues associated with Aluminum, resistivity and electromigration are being seen in the system. Resistivity results in power consumption occurring by the device above the theoretical operational power of the gates. In addition, it results in a delay in the Resistivity Capacitance (RC) delay which is induced by the electrical characteristics of the complete barrier/adhesion layer and metal

line as a complete system. The metal line length contributes to the phenomena. As shown in figure 1, the interconnect lengths can be divided into three different lengths: Local, Intermediate and Global. Local interconnects connect close electrical devices, are very short from line length perspective, and do not have significant RC delay. The intermediate and global interconnects do have considerable length and ultimately can contribute to the overall RC delay, constraining the IC's overall speed and thus are a central concern for device performance. Devices shrink at a fairly constant rate per generation and the generation iteration has historically been on a 2 year interval. Moore's law accounts for this pattern from an economic sense. RC delay per generation can be described via a very simple, general equation: [3]

$$RC = 2\rho\varepsilon\varepsilon_0\left(4\frac{L^2}{P^2}+\frac{L^2}{T^2}\right) \qquad 1$$

Where ρ is the specific resistance, ε is the ILD permittivity, ε_0 is vacuum permittivity, L is the line length, P is the pitch between lines, T is the line thickness. This provides a measure of RC delay scaling which contributes a significant portion to the overall speed of an integrated device.[4] If the lines are too close together, there will be a capacitance delay induced by the coupling of the electrical fields. In addition to the general scaling effect, the continued interconnect shrinking pushes the need to understand how interfaces can contribute to the overall device performance. It has been shown that the sidewall barrier properties are among the single largest contributors to the RC delay at aggressive dimensions.[2, 5] The RC delay becomes more prevalent upon metal lines shrinking as the surface contribution of the electron scatter in the metal line goes up relative to the bulk electron transport. This phenomenon is shown in Figure 3.

In addition to the RC Delay issue, electromigration is a pervasive issue with copper interconnects. Electromigration is a phenomenon that occurs over time and is a critical failure mechanism for IC's.[2, 6, 7] It occurs due to a momentum exchange between electrons and metal atoms. The interaction leads to a net diffusion of metal atoms in one direction. At the cathode end of the line, a void is formed. At the anode end, a metal extrusion forms. This leads to device failure as the interconnect will short to another interconnect or become unconnected. The phenomenon occurs at the surface of the copper and is believed to be driven by copper diffusion at the interface of the adhesion layer or the copper grain boundaries. Better adhesion and greater chemical bond reactivity of the barrier layer to the metal layer is believed to slow the phenomena and could explain early copper interconnect lifetimes being short due to the barrier/liner systems not being optimized.[8]

The scaling of the interconnect system is associated with the interfaces of the system and the complexity of the interconnect system. Research is ongoing to assess other barrier and adhesion layers to eliminate the side wall RC delay and allow interconnect scaling. Another approach is to assess the interconnect system as a composite and attempt to optimize the overall structure, this basically means to not just change the adhesion/barrier layers, but to determine if a change in the metal could enable improved scaling.

The author is assuming that low resistive metals, Copper, Silver or Gold, will provide the best interconnect electrical performance and hence a barrier layer will be needed. The choice of the metal and the barrier layer will be discussed in chapter 2. Before this, a review of what is needed for a barrier layer and stability of an interface should be reviewed.

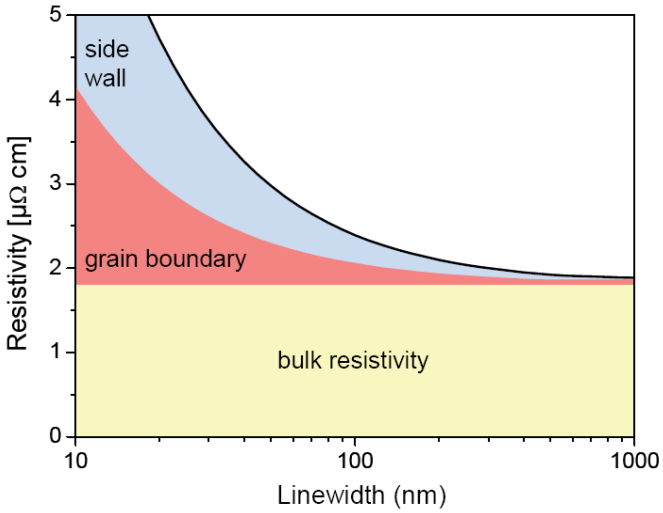

Figure 3. Resistivity scaling of Interconnect lines upon linewidth scaling.[9]

Barrier Layers and Interface Considerations

The properties of nanometer size systems are defined by the interface.[10] A key part of the assessment of a new metal will be if the interconnect system is mechanically stable as a composite and if it can be scaled to the needed dimensions while maintaining mechanical stability, relatively inert from a thermodynamic perspective and its electrical characteristics are unchanged.

Interfaces are the region between two dis-similar substances either in terms of chemical composition, crystal structure or both. An alternative way of interpreting an interface is by considering it a buried structure or defect.[10] The interface is a 2-Dimensional structure and typically contains unique chemical and physical characteristics. The ability of two materials to adhere to each other is not always dictated by their ability to form compounds.[8] The adhesion between a ceramic and a metal is strongly influenced and even dominated by the surface energy and not by the interface energy. In addition, large interface strain or incoherent interface bonding may limit the formation of a stable interface.[11]

A surface can be viewed as a system which has broken bonds. These broken bonds allow for lower energy bonding occurring between species which may not typically react or the reaction maybe sterically hindered due to the constraints imposed by the two surfaces. The interface maybe formed by species which typically interact or by the fact that the chemical constituents of the system want to ensure all of their bonding is complete relative to the preferred state. This is supported by the current barrier layer material choice. Copper is immiscible in tantalum and immiscible in tantalum nitride, but these materials are used as a composite system for interconnects. This highlights the fact that adhesion and chemical reaction are separate phenomena.

One particular problem with heterogeneous interfaces is the lattice mis-match between the two different phases. Epitaxial thin film growth experiments show that the lattice dimensions of the substrate are maintained in the growth film when the thickness is small.[10] This occurs up to a critical thickness value and then the systems stress pulls the film back into the expected lattice dimensions for the thin film. This suggests for *Ab Initio* studies, the "deposited" film should match the lattice of the substrate, or it may result in high residual stress of the deposited thin film. An alternative way of looking at this problem from an interface setup perspective is to increase the size of the small lattice with repeat cells until an alignment can be reached in terms of the atomic alignments.[10] The system could end up having strain relieved and lower interface energy due to atomic voids or atomic re-arrangements.

Barrier layer materials need to have several key properties.[12] First, they have to be thin and stable. They cannot readily react with either the metal or the ILD. Second, they need to be highly conformal to avoid void formation or allow the metal to make contact with the ILD. In the case of copper and carbon doped silicon dioxide (CDSIO), this is very problematic as copper has a high diffusivity rate in CDSIO and will rapidly

cause a short and kill the device. Third, they have to promote adhesion between the metal and ILD to ensure mechanical stability of the interface. Fourth, they need to have good conductance as the metal lines shrink and the total cross section of the barrier layer ultimately takes up a significant percent of the overall metal cross section. The interface of barrier layer and the metal is critical to the composites performance. Now a key question is how to assess such a system.

Methods for Interface Studies

Study of the interfaces is not a trivial task, as one has to first create the interface of interest without defects or experimental issues inducing an unexpected system. Creation of interface systems can occur through advanced, in vacuum processing. These can include various vapor phase deposition techniques. Included in this list are Physical Vapor Deposition (PVD), Chemical Vapor Deposition (CVD) and Atomic Layer Deposition (ALD) techniques. PVD and CVD rely upon evaporation and deposition of atomic species. On can control surfaces, stoichiometry and thickness by modulating input parameters such as gas pressure, temperature gradients and fluctuations in the evaporated species composition. ALD is slightly different as it is step wise chemical buildup of a surface. One would produce precursors that would allow for controlled deposition of systems and eliminate thickness and compositional fluctuations as the precursor chemistry is the control mechanism at the micro level. While these techniques provide the ability to form various thin films at the atomic scale, they have an inherent flaw for early studies on novel concepts. They require significant time and effort to ensure that the correct material crystal structure and composition of interest is the actual one being deposited. Significant changes from a known system require complex

experiments and research time to understand the proper processing conditions. In addition to this problem of sample creation, is the need to actually study the interface. There is a shortage of experimental tools to study interfaces, but it can be studied by analytical means such as Transmission Electron Microscopy, Electron Energy Loss Spectroscopy or Grazing Angle X-ray Scattering to name a few techniques. The techniques are limitation in terms of their abilities to study just the interface as they have to have more material than a monolayer to analyze or cannot access a buried interface as their surface sensitivity is a result of surface stability in ultra-high vacuum environments.[13] In addition, the buried structure maybe metastable and by studying it the interface could allow enough energy into the system to change to a more stable phase or structure.

First Principle or *Ab Initio* modeling offers an alternate way of studying the interface as 1.) All conditions and properties can be controlled, 2.) The specific nature of the interface can be analyzed and 3.) Specific chemical constituents can be accessed. Others have looked at the way systems form interfaces for various carbides, nitrides and oxides. In particular, nitride systems were examined as to how Aluminum would adhere to polar and non-polar nitride and carbide surfaces including Vanadium Nitride, Vanadium Carbide and Boron Nitride.[14, 15] The studies show that the adhesion of the metal surface preferred bonding to the metalloid species (nitrogen or carbon). The work suggests that the work of adhesion should be highest when the metal surface can align to the metalloids on the surface. Siegel goes on to show that polar surfaces are dominated even further by the metalloid which causes the interface to have even greater adhesion when compared to other potential surfaces in the same crystal system[16]

.

An ab initio study into the Interconnect system would provide insight into processing and electrical properties that would allow one to understand what experimental systems may be the best to invest physical research time to study systems further. This study will employ this technique to help understand an alternate Interconnect path.

Summary

The continued scaling and adherence to Moore's Law has pushed the semiconductor device manufacturing into atomic scale systems. By 2022, Interconnects will be 10 nm in width and the barrier layer that ensures the stability of the metal will be 1 nm in thickness. The continued scaling will result in the system being dominated by surface effects. The current, industry standard set of materials used for Interconnects, Copper, Tantalum, Tantalum Nitride, appear to have long term scaling issues including RC delay associated with the interface and electromigration resistance.

The author is proposing to study an alternate metal and barrier layer to determine if there is a better "composite" system one could use for Interconnects. The study will be ab initio based and intended to provide guidance on interconnect direction. The next chapter will provide an overview of what those materials are in the interconnect and where the research will focus for those systems.

Chapter 2

LITERATURE REVIEW OF MATERIAL SYSTEMS

In this chapter, a review of the materials of interest will be provided. The first topic will be on which metal to choose of the low resistance group. There is significant data on Copper and study of an alternate metal could provide insight into whether an industry shift may be needed to overcome copper's inherent flaws as an interconnect metal.

The second topic and higher importance is the selection of the barrier layer material. As the interface of the barrier layer and the metal is dictating the way the interconnect is behaving, careful consideration will have to be given on a system that may provide insight into what might be a good course for a viable, scalable interconnect system.

Metal Interconnects

In the early 2000's, copper was introduced into IC production to replace aluminum. Research and development was on going in the 1990's to incorporate the product. The reasons for the change to copper from aluminum include better RC delay, electromigration and better mechanical properties.[17] Copper offers significantly lower bulk resistivity compared to aluminum and Al alloys.[3, 4] A Copper alloy of Al-0.5%to 1% Cu is typically used in the industry.[18, 19] The alloy improves electromigration performance, films are topographically smoother, and the aluminum forms a protective oxide on the copper.[18] As noted in chapter 1, Copper does have a set of new issues associated with it. It requires a barrier layer as it can diffuse into various ILD materials and short out the device.

The use of silver in this study is based on the fact that it has a lower bulk resistivity than copper and is shown in figure 4.[20] Silver may be a possible future replacement for copper. It should be noted that silver suffers from the same scaling issue as copper with respect to the line shrink, but little effort appears in the literature on engineering of silver as an alternative metal. The publications to date seem to indicate integration issues which could be related to maturity of silver processing. Issues such as material defects and formation of various nitrides and oxides at the interface of the silver metal line and the barrier layer are more indicative of a lack of development effort than a scientific, physical reason the material not to be used.[8, 21-23] In addition, it has been noted that Silver may have the same electromigration issues as copper.[2]

However, copper has seen drastic improvements in electromigration issues due to alloy research. Development of silver alloys could be possible to also overcome the electromigration issues observed in the literature.

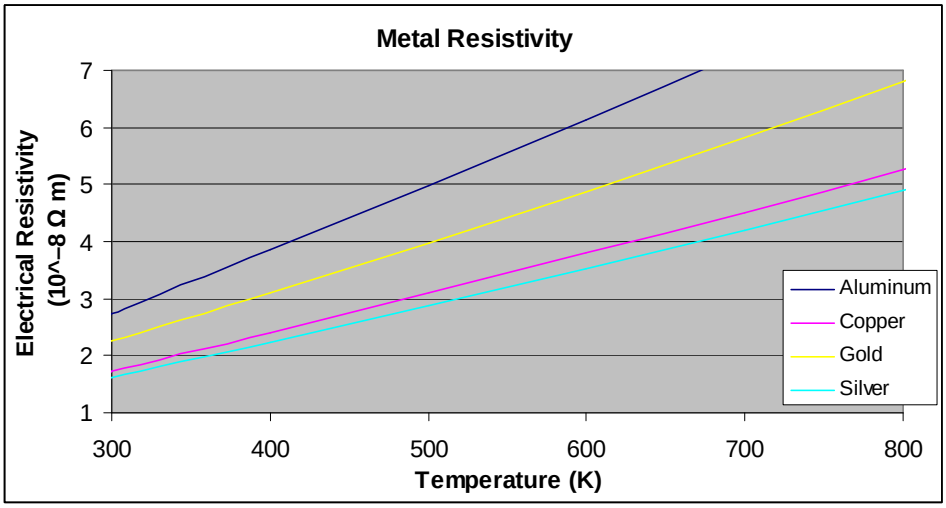

Figure 4. Graph of Metal Resistivity with respect to temperature.[20]

In order for there to be a move to silver from copper as the primary metal for interconnects, there would have to be significant development. The development effort

would require some projected success level to help justify the time and cost investment necessary to enable such a drastic change from copper.

The concept is that silver may have different adhesion properties to barrier layer when compared to copper. In this study, Tantalum Nitride has been chosen as the lattice mismatch between Ag and TaN is smaller compared to Cu lattice when looking at the (111) planes of these metals. Table 2 is provided for reference and shows the various lattice parameters for silver, gold and copper. Silver has the largest lattice constant when compared with gold, copper, or aluminum. In the next section, the crystal structure of Tantalum Nitride will be discussed and the specific crystal structure will be selected.

Table 2. Crystal structure of aluminum, copper, gold and silver.[20]

Material	Lattice Constant (a_0, nm)	Atomic Radius (nm)	Space Group
Silver (Ag)	0.4085	0.144	$Fm\bar{3}m$
Gold (Au)	0.4078	0.144	$Fm\bar{3}m$
Copper (Cu)	0.362	0.128	$Fm\bar{3}m$
Aluminum (Al)	0.405	0.143	$Fm\bar{3}m$

Tantalum Nitride

Typical materials used for barrier layers and adhesion layers are tantalum nitride and tantalum, respectively. The TaN:Ta system is indicated in numerous studies and experimentally seems to be a good choice as it has high thermal stability, low electrical resistivity, and low diffusivity for copper. The standard process currently uses CVD or PVD deposition for the TaN and Ta. The deposition technique and conditions will dictate the crystal phase and stoichiometry of the layers.

TaN will need to be deposited by Atomic Layer Deposition (ALD) at these aggressive dimensions.[12] The crystallographic characteristics of an ALD film are strongly dictated by the precursors and the processing conditions used for the film

creation. The literature currently lists the cubic phase of TaN being deposited, but there is no reason that the thermodynamically more stable CoSn phase of TaN could not be deposited and more importantly that it is not used in modern IC devices as the actual crystal structure used in production devices is publically known.[12] In addition, ALD starts from organo-metallic or halide-metallic based precursors which may leave defect centers such as carbon, vacancies, or halides at the system interface.[2]

The phase diagram for TaN is shown in Figure 5. The 1:1 stoichiometric CoSn phase is thermodynamically stable up to relatively high temperatures and the crystal structures with regions of thermodynamic stability for TaN are CoSn and NaCl, with Ta_2N having the NiAs phase. The tantalum-nitride systems has a significant number of poly-morphs and at least 3 poly-morphs at varied conditions for the 1:1 stoichiometric compound and are listed in Table 3.[24]

There are few first principle studies of the Ta_xN_y polymorphs and fewer include the CoSn phase. The studies are listed in Table 4 with calculation information extracted from the publications. Table 5 provides the statistical overview of the *Ab Initio* studies of the 1:1 stoichiometry TaN systems and reported values for various parameters including lattice constants, heat of formation, and bulk. While there are reports of CoSn and NaCl phases being thermodynamically stable and preferred[25, 26], there are other reports of thermodynamic stability of some stoichiometry's (Ta_5N_6 and Ta_3N_5) that do not occur in the published phase diagram.[27, 28] The stable phases from these studies are NiAs-Ta_2N, Ta_5N_6, Ta_3N_5 and WC-TaN phases. [26-28] In addition, the NaCl and CoSn are proposed to be meta-stable from first principle calculations.[27, 28] Experimentally, WC phase is formed by compression of CoSn Phase.

There could be several reasons for the discrepancies between the experimentally derived phase diagram and the *ab initio* determined stable phases. For the *ab initio*

studies, two points of concern: Entropy and improper system setup. Entropy may impact the final phase as shown in the phase diagram. The studies show small enthalpy differences between phases[27, 29], and entropy effects were generally not included, so the calculated results are mostly relevant to zero Kelvin.

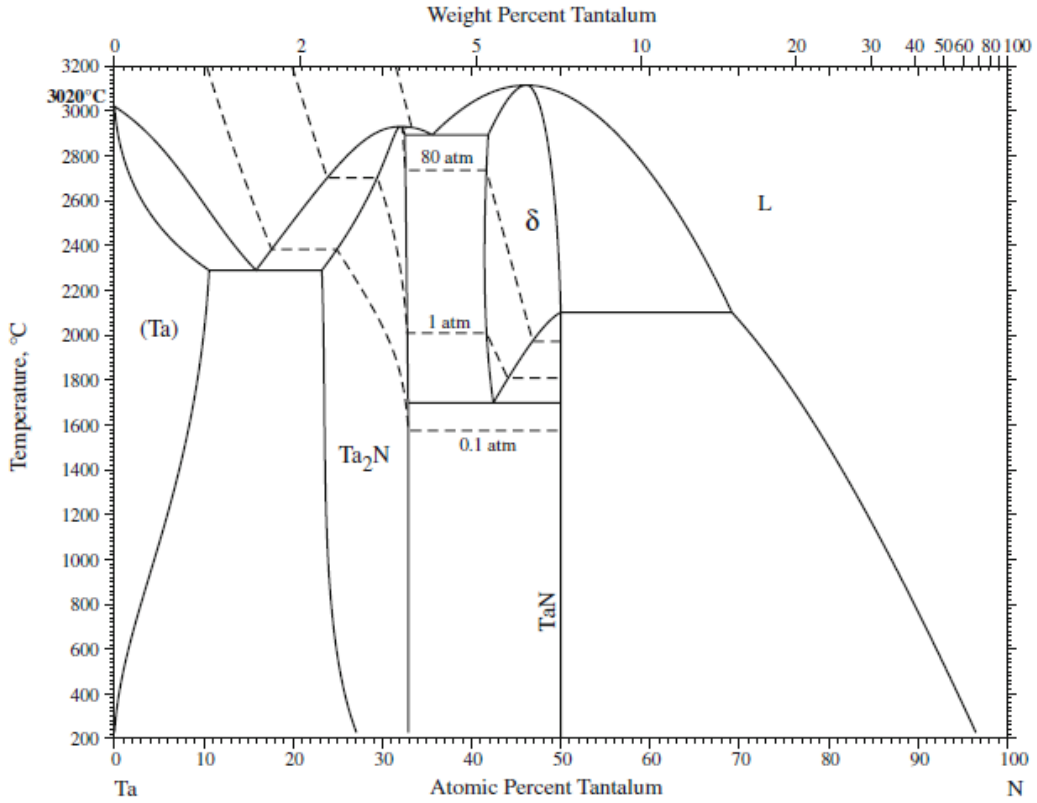

Figure 5. Phase Diagram of Tantalum Nitride.[1] Ta_2N type Fe_2N structure. Tantalum occurs in a BCC structure; TaN is the CoSn phase and δ is a 1:1 NaCl cubic phase.

For improper system setup, the parameters as noted in the publications are listed in Table 4 as to highlight gaps in individual studies. Only one study uses the correct gamma centered k point schema. This would result in a poor convergence of the systems as the incorrect space sampling will occur. In addition, the published studies seem to lack all needed details to repeat their work properly. A summary of the overall published ab initio studies of the stoichiometric TaN compounds is also shown. The three standard phases of TaN (WC, CoSn and NaCl) are shown to provide a guide as to the extent to

which the systems have been studied. Comparison across the result sets will be done upon completion of the work in this dissertation, but the results seem to suggest fairly good calculation convergence for lattice parameters across phases, but few studies look at the stability or modulus of CoSn and the WC phases. These crystal structures are more sensitive to proper convergence when determined via first principles.

Table 3. Table of Tantalum Nitride Polymorphs [24]

Phase	Stoichiometry	Structure/Comments
α-TaN	$TaN_{0.04}$	N in BCC-Ta
β-TaN	$TaN_{0.05}$	Same as α-TaN
γ-TaN	$TaN_{0.5}$	HPC Ta w/ N Atoms occupying half of octahedral sites
ε-TaN	$TaN_{1.0}$	HPC, CoSn
δ-TaN	$TaN_{0.92-0.97}$	FCC-NaCl
Θ/ν-TaN	TaN_{1}	HPC-WC, formed from CoSn under high pressure
Ta_5N_6	$TaN_{1.2}$	Hexagonal
Ta_4N_5	$TaN_{1.25}$	Tetragonal
Ta_2N_3	$TaN_{1.5}$	Fluorite structure with N vacancies
Ta_3N_5	$TaN_{1.66}$	Orthorhombic, Fe_2TiO_5

The results of the *Ab Initio* studies do provide guidance on the electrical characteristics of Ta_xN_y. Ta_2N has been shown to have strong metallic nature initially, but with increasing nitrogen, the resistivity increases until it finally transitions to insulating.[27] The N-rich structures were found to have dramatically increased resistivity once beyond the 1:1 stoichiometry.[30] Once past the 1:1 stoichiometry, increasing N content results in decreased barrier performance.[26] The incorporation of nitrogen helps in one of two ways: First it results in nano-size to amorphous crystal formation which helps to delay the formation of larger grain, polycrystalline TaN. The second way the excess Nitrogen helps is to delay the rate of diffusion of Silicon into the TaN from the other side. Overall, this improves electromigration performance.[31]

While there are numerous polymorphs for TaN, there is another phase that is suggested in the literature both in ab initio studies and in experimental studies. In 1978, Christensen suggested that the correct crystal structure of the 1:1 TaN was not the CoSn

phase, but a Fe_2P crystal structure.[35] The first study was done using x-ray diffraction and Christensen suggested that the original analysis done was limited as x-ray diffraction predominately occurs from the Tantalum atoms. The author assessed the crystal structure using Neutron diffraction and thus allowed an increase in the positional information of the Nitrogen. The author was able to show that the structure was not CoSn, but Fe_2P.

Table 4. Table of *Ab Initio* Studies run on TaN in CoSn phase. EX is the Exchange Correlation Functional

#	PP	EX	Code	CoSn Studied	k point (CoSn)	K point schema	Ref
1	FLAPW	LDA		Yes		MP	27
2	FLAPW	LDA		Yes		MP	30
3	US	GGA	VASP	Yes	15x15x11	MP	32
4	US	GGA-PBE	ESPRESSO	Yes	8 × 8 × 14		25
5	PAW	LDA	VASP	Yes	845 to 4913	Gaussian	29
6	PAW	GGA-PBE	VASP/ CASTEP	Yes	7x7x11	MP	33
7			VASP	Yes	6x6x10	MP	26
8		GGA	DMol	Undefined			34

Table 5. Published *Ab Initio* summary statistics

Item	system	Lattice Constants (nm)		Bulk Modulus (GPa)	Cohesive Energy (eV/TaN Unit)	Heat of Formation (eV/atom)
		a	c			
Count	CoSn	4	4	2	1	5
	WC	4	4	3	0	3
	NaCl	9		6		6
Min	CoSn	5.16	2.89	251	-14.046	-1.49
	WC	2.91	2.86	337		-2.73
	NaCl	4.33		327.6		-1.95
Max	CoSn	5.30	3.18	303.6	-14.046	0.21
	WC	2.95	2.90	384	0	-2.35
	NaCl	4.42		403.9		-1.00
Mean	CoSn	5.23	2.97	277.3	-14.046	-0.87
	WC	2.93	2.88	352.7		-2.48
	NaCl	4.37		360.2		-1.50
1 σ	CoSn	0.06	0.13	37.2		0.65
	WC	0.02	0.02	27.1		0.22
	NaCl	0.04		30.8		0.36

In 2011, an *ab initio* study also looked at the enthalpic stability of the NaCl, CoSn and Fe_2P phases. The work suggested Fe_2P was more stable enthalpically than CoSn. In addition, the Energy vs. volume curves showed that the Fe_2P was lower in enthalpy than the NaCl phase. This coupled with the Neutron diffraction study, suggests that the Fe_2P phase is the correct one. As noted above, the CoSn phase has been noted as having lower stability when compared to other polymorphs of TaN. In addition, as researchers have been analyzing CoSn as the correct phase, there has only been 3 studies noting Fe_2P phase as a more stable crystal structure and running simulations with this understanding of crystal structure.[26, 28, 36] There is no crystal defect data on the phase or ab initio study on surface of Fe_2P-TaN. In Figure 6, the amount of motion expected in the nitrogen's is shown. Only the basis set is drawn and the arrows show the direction and amount of shifting of the Nitrogen's when going from the CoSn phase to the Fe_2P phase.

Few studies have analyzed the interface of CoSn-TaN phase with respect to a metal.[32, 34] The interface strain energy was shown to be lowest for the (001) TaN-CoSn and the (111) copper interface at 0.01 eV/atom compared to the (111) Cu interface and (111) NaCl-TaN, (001) Ta_2N, and (110) BCC-Ta which had 0.33 eV/at, 0.33 eV/at, and 0.26 eV/at, respectively.[32] The interface strain is associated with how much the two crystal structures need to deform to align to adhesion sites at the interface. Cohesive energies are lowest for the Cu-TaN-CoSn interface with the Tantalum rich (0002) interface and the (111) Cu interface with the copper's sitting on top of the Tantalum's. Compared to other crystal structures, the CoSn seems to have similar energies with the order of cohesive energy from highest to lowest for the copper (111) interface being TaN-NaCl>Ta>TaN-CoSn, but separated by < 0.7 J/m^2.

For a mixed surface (tantalum and nitrogen), it was shown that the copper atoms prefer to sit on top of nitrogen atoms for the (0001) surface of the TaN-CoSn phase and Copper forms strong ionic bonds with the Nitrogen. For the tantalum terminated surfaces, copper atoms either take the bridge sites or form bridge sites to form an interface that is a mixture of metallic and covalent bonds, thus the copper lattice forms a mixture of the lattice. Another study has no information on crystal structure of the system analyzed, but did utilize PVD for deposition of the TaN. The study suggests the need to match cohesive energies of 2 materials and why the current barrier-adhesion (TaN-Ta) layer is used today. However, the work does show that a TaN-Cu stack survives the mechanical testing.[34]

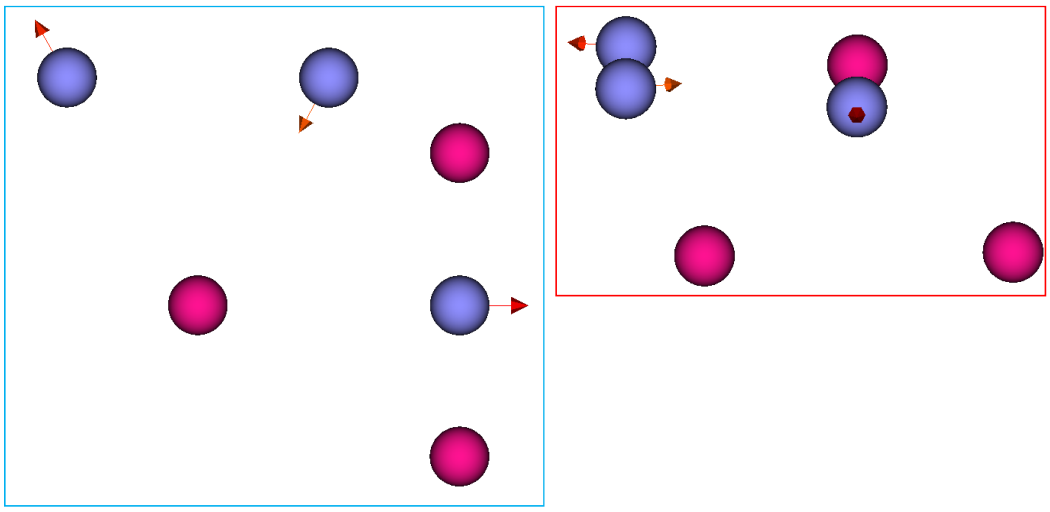

Figure 6. Figure of the atomic movements of Nitrogens ( ) and Tantalums ( ). The arrows show the basis atom movement direction and magnitude of movement to scale. The left, blue box shows the (0001) and the right, red box shows the (0010) with a slight rotation to allow one to see all atoms.

Interface adhesion of the metal with a metalloid terminated ceramics is stronger for polar interfaces and metal atoms located on metalloid atoms have strongest adhesion for non-polar surfaces.[10] Matching the adhesive strength and cohesion strength allows for the barrier layer to be optimal.[34] Layer matching in a multilayer stack along with

composition control have been shown to achieve this match both experimentally and from models. This is a primary reason why multistacks are used in a IC process. Models can be used to screen barrier layer selection by analyzing the adhesive and cohesive energy trends for various barrier layer metallization schemes. This dissertation will focus on the ambient phase (CoSn or Fe_2P) as phase diagram indicates stability. This particular structure has limited studies and there is no known study on the surface/interface of the system.

Research Goals

The published phase diagram suggests CoSn as the ambient forming crystal structure at a 50/50 Ta:N composition. This is both supported and negated by studies by others.[25-27, 36] This dissertation will attempt to assess which crystal structure is the stable one from ab initio studies and determine if other crystal structures are metastable. The work will then use the thermodynamically favorable crystal structure to assess the viability of the silver interfacing with the preferred, ambient crystal structure surface. If the calculations show that the system has both favorable absorption and adhesion enthalipies, then an interconnect with silver and a stable Tantalum Nitride barrier should be considered as an alternate for future interconnect systems. Further experimental study will be needed to validate the conclusions of the work, but the fundamentals of the interconnect will be shown. In addition to overcoming the limitations of the scaling of the current multilayer interconnect systems, the Silver:Tantalum Nitride system may provide an easier, more cost effective interconnect system for the IC industry as a whole step in the process flow is eliminated with the removal of an adhesion layer. For this assessment, as mentioned previously, ab initio methods will be used. This reduces the experimental burden and provides a path to disposition options. The next chapter will

review the Density Functional Theory used to study the system. Chapter 4 will review the Bulk Studies of Tantalum Nitride. Chapter 5 will analyze vacancy stability in the Tantalum Nitride to understand the phase stability further. Chapter 6 will assess the Adatom and adhesion properties of silver on the stable Tantalum Nitride phase.

Chapter 3

AB INITIO THEORY

First Principle studies are based on Quantum Mechanics which was proposed and developed by Schrödinger. The basis of the theory is that a system is defined by its wave function and the Schrödinger Equation can describe how matter behaves[37] The time independent Schrödinger Equation is given [38]

$$H\Psi_k(q_1, q_2, \ldots q_n,) = E_k \Psi_k(q_1, q_2, \ldots q_n,) \qquad 2$$

Where H is the Hamiltonian, E_k is the Eigen values, q_i are the subatomic particles, and Ψ is the Eigen functional. The Schrödinger Equation has 3N spatial coordinates for each N interacting electrons of a system and 3M for each ion leading to 3N+3M variables. The Schrodinger calculates an Energy based on the Hamiltonian operator.[39, 40] The particles interact pair wise and expansion of the Hamiltonian is given by the following equation:

$$H = \frac{-\hbar^2}{2m_e}\sum_i \nabla_i^2 + \frac{-\hbar^2}{2M_I}\sum_I \nabla_I^2 - \frac{1}{2}\sum_{i,I}\frac{Z_I e^2}{|r_i - R_I|} + \frac{1}{2}\sum_{i\neq j}\frac{e^2}{|r_i - r_j|} + \frac{1}{2}\sum_{I\neq J}\frac{Z_I Z_J e^2}{|R_I - R_J|} \qquad 3$$

The first two terms are the kinetic energy of each electron and ion, respectively. The next 3 terms are the electron-electron, electron-ion, and ion-ion interaction terms, respectively. Schrödinger Equation cannot be solved analytically except for the simplest system. However, it can be approximated numerically thus numerical techniques can provide an approximate solution.

A key theorem that enables such numerical techniques to be computationally tractable is the Born-Oppenheimer Theorem.[38, 41] The theorem states that since there is

such a large discrepancies in the mass of the electrons and the nucleus that the two are effectively decoupled with respect to motion. Electrons are dragged by the nuclei and electrons do not affect the motion of the nucleus. This effect can be seen in the rate of motion of the particles with electrons moving at 1 femtosecond and atomic vibrations (nuclei motion) occurring on the order of 1 picoseconds.[41, 42] This reduces the complexity of the Schrödinger equation to a 3N many body problem. A further reduction in the complexity was attempted by others.[14, 37, 43] Hartree is based on a central field theory which can be easily explained by electron screening and proposed a single, non-interacting particle calculation. It would suggest that the electron farthest from the ionic core would only sense a partial charge as the rest of the inner electrons would just result in the total potential field being lowered. The pairwise interactions of the electrons are reduced to a mean field. A major issue with Hartree is that it ignores Pauli exclusions and could allow two electrons to occupy the same spin state.

Hartree-Folk (HF) was built off of Hartree. It accounts for spin and imposes Fermi-Dirac statistics on the electrons. The calculation requires the energy calculation of each individual electron and also handles exchange. Electrons all are attempting to get to their lowest energy states in an atom. They will move in unison and will increase their kinetic energy if it means their potential energy is reduced. This effort is called exchange. These two techniques impose single particle wavefunction in their calculations. An early example of this was the work by Thomas-Fermi-Dirac, but Kohn created the modern day theorem allowing density functional theory (DFT) to be used to solve the Schrödinger equations in a computationally attainable manner.

Density Functional Theory

The Hohenberg-Kohn (HK) theorem and the Kohn-Sham (KS) equations define the DFT method, and Kohn is considered the father of the technique.[37, 43] In 1964, the

HK theorem was developed and states the system energy is a functional of the charge density and therefore the ground state (GS) charge density is the systems ground state energy.[37, 39, 41, 44] The ground state functional can be inverted, allowing ground state observables to be functions of the ground state functional. There are 4 parts to the theorem:

1. Non-Degenerate ground state wave function is unique to the ground state density

2. The key observable is ground state energy and the system energy can never go below the ground state

3. Kinetic and interacting energies of non-relativistic coulomb systems defined by universal operators on that system.

4. If density functional is held fixed, by determining GS wave and potential of the system is known. (i.e. the whole system Hamiltonian is known)

This method was adapted to determine the Eigen states of the KS Hamiltonian. To minimize the ground state energy the sum of the kinetic, interacting and potential energies should be minimized.

The implementation of DFT is done by the Kohn-Sham (KS) Equation.

$$-\frac{\nabla^2}{2}\Psi_i(r)+v_{KS}[n](r)\Psi_i(r)=\varepsilon_i\Psi_i(r) \qquad 4$$

Where Ψ are the Eigen functional and v_{KS} is the KS potential. The Kohn-Sham equation transforms the many body problem to look like a single particle orbital problem.[37, 39] The basis set is used to expand the KS Eigen Functional and can be classified by either plane wave or local basis sets. This allows single particle theory to be applied, but leads to the need to apply exchange correlations to describe the interactions of the electrons in the system. No "direct" exchange correlation functional exists, so approximations have been

developed to describe the atomic interactions. The exchange correlation functional will determine the calculations physical "accuracy" and all other computational specifics of the simulation will determine the numerical aspects of the calculation.[39] The KS potential (ν_{KS}) is defined to have the following terms and is acting on the electron density (n).

$$v_{KS}[n](r) = v_{ext}(r) + v_{Hartree}[n](r) + v_{xc}[n](r) \qquad 5$$

The $v_{xc}(r)$ is the exchange-correlation functional of the equation, v_{ext} is the external potential (nuclei), $v_{Hartree}$ is the Hartree potential.[45]

Exchange-Correlation

There are several methods to estimate the exchange correlations energy. The first approach is called Local Density Approximation (LDA), in which the exchange-correlation energy of each local region of space is estimated to be equal to the exchange-correlation energy of a uniform electron gas of that density (which can be solved exactly). V_{xc} in LDA from the ν_{KS} equation is only defined by the local density of electrons with a total electron density assigned to the whole system and the Kohn-Sham equation is then solved self consistently.[45]

The second approach is the Generalize Gradient Approximation (GGA). The general difference between GGA and LDA is GGA includes both the local electron density and its gradient in estimating the exchange-correlation functional. There is only one LDA, but there are many types of approximate GGA's. The LDA, GGA-PW91and GGA- PBE are well established exchange correlations.[43, 45, 46] There are additional methods such as Meta-GGA and Hybrid, but these are beyond the scope of this paper and can be found elsewhere. [43, 47]

LDA and GGA appear to over and under estimate parameters. LDA overestimates the bonding energy and leads to lattice parameters that are too small by a few percent when compared to experiments and over estimates the cohesive energy. GGA underestimates the bonding energy which leads to lattice parameters being overestimated and cohesive energy being underestimated by approximately the same percent that LDA calculates.[43, 45, 48]

Planewave Basis Set

There are two typical methods to represent the single particle wavefunctions: Atomic Orbital and Planewave. The Atomic Orbital (AO) actually represents the local charge density and one has to predefine the basis set used for the calculation. AO's are good for quantum chemistry simulations as the molecular orbital often look like atomic orbital and defining them can often be done with a few functions. It is very hard to ensure the basis set is complete and not selecting the proper AO's can severely limit the calculation accuracy and the convergence would be incorrect if the basis set is incorrectly defined.

Planewave Basis sets do not need to be defined a prior as do AO basis sets. They are orthogonal and are complete by themselves. The user sets a cut-off energy that defines the number of the planewaves, which affects the accuracy of the calculation. The calculations of planewave basis sets are executed rapidly in modern day code due to the ability to utilize Fourier Transfer Functions from real to momentum space allowing rapid calculation of the potential and kinetic energies. However, the control of the exchange calculation needs to be carefully considered.[43]

One example is they place charge where there may be no charge due to the calculation methods. With that said, PW and AO have been shown to result in the same

ground state energy. This dissertation uses PW's for all calculations, so all further analysis will assume them. One reason to select PW's is due to their ability to represent crystalline materials as one can consider them an infinite slab.

Periodic Boundary Conditions and K Space

An infinite slab allows Periodic Boundary Conditions to be implemented via Bloch's theorem, and the periodic part of the wavefunction can be expanded in a discrete set of PW's in reciprocal space. The periodicity allows one to look at a single cell which replicates and thus you can ignore the infinite slab issue, but requires one to work in inverse space which brings up how to setup the proper K points.[43, 49, 50]

K points are the points chosen in inverse space and the correct choice of k points is tied to the crystal symmetry. The k points can be reduced so that they only calculate symmetrical points. The standard method for this is to use a Monkhourst and Pack method to select a reduced set of points for the analysis. MP will assume a centering of the cell and samples in space from that assumption. It has been shown that MP grids will not converge if not centered on the Gamma point for hexagonal crystal structures.[47]

Pseudopotentials

Pseudopotentials are commonly used to simplify the problem by replacing the core electrons with Pseudopotentials which approximates how the core electrons interact with valence electrons. This can often be a very good approximation because most chemical bonding primarily involves only the valence electrons.[11, 43, 45] This reduction is needed also to make larger systems computationally tractable as it can allow one to treat a high atomic number species in a similar manner as a smaller one with respect to the number of electrons that need to be included in the calculation. From a precision

perspective, the impact to the calculations is minimal when comparing a complete electron system to a valence electron system and is on the order of 1000th of an impact to the system if the valence electrons are only used in the calculations[11], for cases involving typical chemical bonding at thermal energies. However, if atoms move too close together, then the core electrons can also be involved in chemical bonding, and then all-electron calculations are needed. In general, the replacement of core electrons with Pseudopotentials allows a reduction in the planewave sets and thus improves computational time.

The Pseudopotentials have several implementations with Ultrasoft-pseudo potentials and projected augment wave (PAW) potentials being two common types. Ultrasoft potentials are easily used to describe 1st row elements and system with d-/f - electrons are feasible. The PAW potentials take into account nodal features of the valance electrons and are orthonomal.[43, 50] In this dissertation, only PAW potentials are used as the size of the elements are large. The correct metric for how well a PAW potential is constructed is to validate it with the full-potential linearized augmented plane wave (FP-LAPW) and determine how well the PAW reproduces the FP-LAPW results. It has been shown that PAW and FP-LAPW reproduce simple atomic constants to <2% of experimental data and in some cases, the FP-LAPW is out performed by as much as 1% by PAW implementations in VASP.[43, 51]

Energies and Forces

Static DFT calculations are run where the ionic cores are not allowed to move. This is basically an electronic density minimization. This study is interested in atomic movements and thus needs to be able to reliably determine ionic locations. Ionic movements can also be allowed in DFT studies. This requires the determination of the

forces and resulting movement of the ions. VASP uses the Hellman-Feynman Theorem to do this and is based on knowing the gradient of the electronic density relative to the ionic species. The implementation for the theorem works in an iterative manner where the ground state energy is calculated, the force on the ions are determined and then the ions are moved in the direction of the force and then the process is repeated.

VASP Implementation and Reliability

The software used is the Vienna Ab Initio Simulation Package (VASP4.6) developed by Georg Kresse, Martijn Marsman, and Jürgen Furthmüller at the Universität Wien, Austria. VASP is implemented with a planewave basis set for single particle Kohn-Sham wavefunction along with PAW Pseudopotentials to describe the electron-ion interaction for more complex orbital systems.[52, 53] Ground state electron density and energy are calculated with a conjugate gradient method. The cell stress and forces acting on the ions are determined by Hellman-Feynman method augmented with a Pulay stress calculations with minimization done by a quasi-Newton method.[43] The exchange correlation functional used in this dissertation for bulk calculations are Local Density Approximation (LDA), Generalized Gradient Approximation Perdew Wang 91 (GGA-PW91) and Generalized Gradient Approximation Perdew Burke Ernzerhof (GGA-PBE) exchange-correlation functionals.[54, 5554-59] The defect cell and surface slab was only analyzed with the GGA-PBE to save on computational time. The defect and surface/Adatom calculations used GGA-PBE and used the planewave increased by 30% to help ensure proper convergence and avoid Pulay stresses. The analysis as to why GGA-PBE will be discussed later after bulk calculations. The lattice constants calculated in the bulk calculations were used as input values to the defect and surface calculations.

The calculations are divided up into three parts: Bulk calculations, Defect calculations, and Surface/Adatom Calculations. The flow was as follows for each of the calculations and crystal structure analyzed in the thesis:

1. Build cell using experimental lattice constants
2. Select a reasonable K space and increase k-space until the change in energy per an atom is less than 10 meV/at, unless otherwise noted for the calculation. Use the smallest K space for future runs.
3. Increase planewave cut off and monitor convergence of the energy until < 10 meV/at.

DFT has been implemented in several codes similar to VASP (Quantum Espresso, Abinit) and there are slight differences between the implementations. Ultimately, the theory of DFT needs to be correlated to real world experiments. The simulation results must come predict the results seen in the experimental world. If the DFT simulation is correctly done and the error of the real world experiment is controlled, it has been shown that the techniques result in close agreement.

DFT studies have been increasing significantly in recent years. A quick survey of publications in the academic space by looking at Web of Sciences shows a significant increase in the publications in the space and shown in Figure 7. The graph is a cumulative total of publications based on Web of Science data. This suggests a growing number of researchers using the tool, but not necessarily the quality of the data or of its relevance to the experimental world. For this, I will look at a few review publications. For instance, crystal lattice constants have been tabulated by Hafner and suggest that VASP is capable of matching experimental and theoretical to within 1% of each other.[43]

Mechanical properties show better than 10% to experimental values both by Hafner and Mavromaras.[43, 60] In addition, Adatom absorption energies have been calculated to within 0.5 eV of experimental values with the GGA-PBE.[43]

As mentioned, the results of simulation studies have to be carefully assessed as to the real world implications and analysis. Throughout the dissertation, references to experimental values will be provided an assessed to the simulated results when possible. These should be used as a guide to the validity and reliability of the results provided where there is no such experimental data or where the experimental data is not clear.

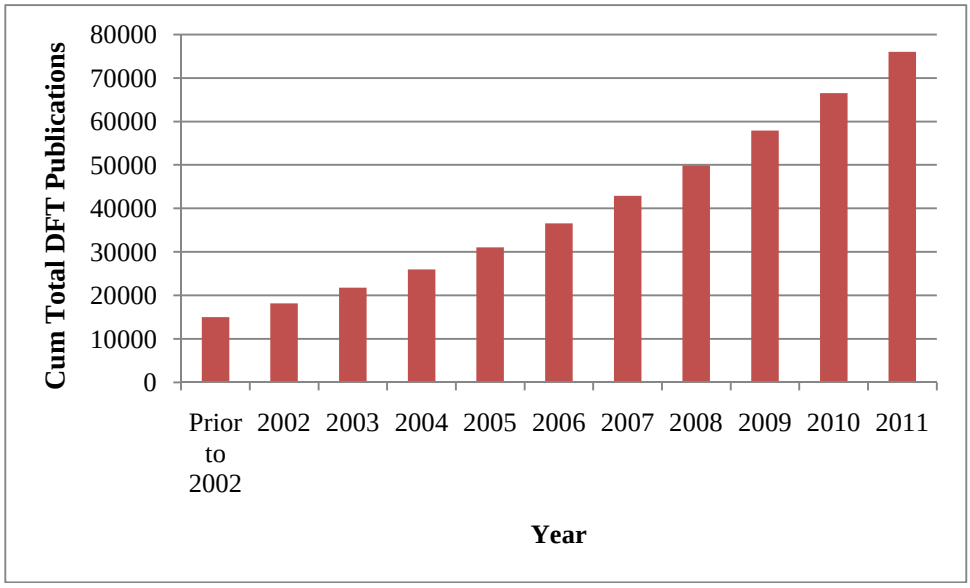

Figure 7. Total publications on Density Functional Theory as determined by performing a search on Web of Science.

Geometry

The calculations looked at include several different crystal structures and are captured in table 6. The Tantalum Nitride was analyzed in a NaCl, CoSn, and Fe_2P phase. For the CoSn and Fe_2P phases, K space was centered on the gamma point to ensure k point symmetry was properly accounted for in the calculations. Isolated atoms of Ta, N, Ag and Cu were run in a larger isolated box. The Tantalum Bulk calculation as

done a BCC structure. Calculations of Silver and Copper were done on FCC structures. The crystal structures were visualized with either VMD or Visit.[61, 62]

Table 6. Table of the various crystal phases used in this study.

	Space Group	International Symbol
NaCl-TaN	225	$Fm\bar{3}m$
CoSn-TaN	191	P6/mmm
Fe2P-TaN	189	$P\bar{6}2m$
Tantalum-BCC	229	$Im\bar{3}m$
Nitrogen Gas	NA	NA
Silver-FCC	225	$Fm\bar{3}m$

Charge Density Plots

The Charge density of the Bulk systems was calculated and provides insight into the distribution of charge for the system. This is done by DFT calculations by assigning a grid to the system and then overlaying the charge at each point as determined at the ground state. It is then visualized by either contour plots or 3-D isosurfaces. The plotting of the system allows one to see where electrons and charge reside and thus where bonding is occurring. Historically, plotting of charge was an issue as the core electrons typically would have large values associated with them from a density perspective. In the implementation used, only charge associated with the valance electrons is provided as PAW's only include these electrons and therefore the core electrons will not obscure the plots.[50, 63]

Density of States

The density of states (DOS) is a count of the total number of states electrons occupy or can occupy by energy level. It provides insight into how the system is bonding, but needs to be carefully analyzed in doing so. Once the eigenfunctions (states) and eiganvalues (energy) are known for a particular system, one can construct the DOS.

By looking at the point where the Fermi-energy occurs, one can distinguish the overall systems characteristics and whether a system is a conductor (i.e. metallic in nature) or an insulator (i.e. semiconductor or dielectric). If the Fermi-energy lies in a region where there is no states present and between two peaks in the spectrum, the material is either semiconducting or a dielectric. The separation of the peaks determines if the system is one or the other (i.e. large separation is dielectric, small separate is semiconductor). If there are states occurring in the DOS spectrum, then the material is metallic. To compare different system on a graph, it is common to re-align the energies of all systems to their Fermi-Energy.[63]

Electron Localization Functional

The Electron Localization Functional (ELF) provides a way of understanding the location of an electron. It is a scalar quantity between 0 and 1 which has a value of 0 for a vacuum (perfect insulator) 0.5 for a metallic bond and a value of 1 for a covalent bonding. It will provide how the electrons are populating the spaces in terms of Pauli exclusion. The function for the ELF calculation is as follows

$$ELF = \frac{1}{(1 + \frac{K(r)}{J(r)})^2} \qquad 6$$

Where K(r) is the Pauli Exclusion Kinetic energy at some distance, r and J(r) is the Kinetic Energy of a homogenous electron gas at the same point in space. The function is plotted over top the ionic locations to understand where electrons are paired or not.[50] The function is visualized to help understand how the ELF fills space and then assessments can be done to understand how bonding is occurring in a system.

Bader Analysis

A common method to do charge transfer analysis is called Mullikan analysis. Mullikan analysis needs to have the basis set localized on the ions. In Planewave based calculations, such as those used in this dissertation, the plane waves are not associated with a particular ion in the system. So, the traditional Mullikan analysis is not possible.[64]

An alternate analysis is to use the charge density of the system and divide the system up into a grid. By then analyzing the planes to see where there is effectively no change in the density of the electrons going from one point to the next, one can segregate out volumes. These volumes are called Bader regions. The bader regions can then be assigned a charge based on the total charge in that volume.

Algorithmically, this is quite simple and the quality of the results is heavily dictated by the incoming grid. Original algorithms would preferentially trace the lattice and result in erroneous division of the bader region. Tang has corrected this anomaly by two means, 1 increasing the space grid sufficiently to ensure the charge gradient can be determined and also by interpolating slightly off the grid of the charge density.[65]

This results in the systematic error for simple ionic systems such as NaCl having charge assignment errors < 0.01 e.

The use of DFT is a very valuable tool for studying materials. The calculations provide access to the ground state energy on bulk crystals, surfaces of crystals and interface structures. The ground state energy is the enthalpy of the system at zero Kelvin and then by applying various analysis techniques, it is possible to explore various material systems and propose further research either via additional experiments or simulations.

Chapter 4

AB INITIO STUDIES OF BULK TANTALUM NITRIDE

This chapter of the dissertation provides clarity to which of the 1:1 stoichiometric phases of Tantalum Nitride are thermodynamically stable at ambient conditions. DFT is used to calculate the lattice parameters; bulk modulus and Heat of Formation of TaN in the NaCl, CoSn, and Fe_2P phases using 3 types of exchange correlation functionals. In addition, the Density of States (DOS), Electron Localization Functional (ELF) and Bader analysis were calculated and provide insight into the bonding between the Nitrogen and the Tantalum. Vacancy formation enthalpies for NaCl-TaN CoSn-TaN and Fe_2P-TaN are calculated to help understand phase stability and composition range.

The *Vienna Ab-initio Simulation Package* (VASP 4.6) was used to perform the calculations. The bulk systems used Localized Density Approximation (LDA), Generalized Gradient Approximation Perdew Wang 91 and Generalized Gradient Approximation Perdew Burke Ernzerhof (GGA-PBE) exchange-correlation functionals.[54-59] Projector augmented wave Pseudopotentials were used to describe the core electrons, and the valence electron wave functions were described with a plane wave basis set cutoff of 400eV for the perfect crystals[52, 53] The 3 phases are CoSn-TaN (Space group: 191; Short international symbol: P6/mmm), Fe_2P-TaN (Space group: 189; Short International Symbol: $P\bar{6}2m$) and NaCl-TaN (Space group: 225; Short International Symbol: $Fm\bar{3}m$). CoSn-TaN and NaCl-TaN are documented on the phase diagram.

Bulk Studies Calculations Methods

The published, experimental lattice constants were used to initiate all bulk studies, and were optimized by analyzing the energy vs volume curves. As the CoSn and

Fe_2P phases are HCP, the choice of a and c were done to ensure that both directions were changed by the same amount. The k-space was 15x15x13 and 9x9x9 for hexagonal phases (CoSn and Fe_2P) and NaCl phases, respectively. Systems were converged to <1 meV/at. The k space was gamma centered for CoSn and Fe_2P to avoid issues with the symmetry of the K space and convergence issues. The NaCl phase K point schema followed the standard Monkhorst Pack method. All three kspaces were generated using the Monkhourst Pack method. The Volume and associated ground state energy of the systems was calculated and fitting to a third order polynomial for minimal calculations.

Bulk Modulus, Heat of Formation and Cohesive Energy were calculated for the CoSn, Fe_2P and NaCl phases. The isothermal bulk modulus (B) can be defined by this equation of state (EOS):

$$B = -V\left(\frac{\partial P}{\partial V}\right)_T \qquad 7$$

Where V is the volume of the material, P is the pressure applied to the material at a specified temperature. The equation assumes the material responses in a linear fashion regardless of the applied pressure direction. The Murnaghan Bulk modulus EOS was used in this dissertation with the cell volume modulated by ± 1%.[66]

$$E(V) = E_0 + \frac{B_0 V}{B_0^{'}}\left(\frac{\left(V_0 / V\right)^{B_0^{'}}}{B_0^{'} - 1} + 1\right) - \frac{B_0 V_0}{B_0^{'} - 1} \qquad 8$$

Where E_0 is ground state energy, B_0 is the bulk modulus at the ground state, V_0 is the ground state volume and V is the system volume. B'_0 is value of the bulk modulus first derivative value at the minimal energy. The numerical approach to solving this is as follows:

1. Vary the size of the unit cell by a few percent. In the case of a HCP cell, the unit lattice constants of a and c need to be varied independently.

2. The resulting curve of Energy vs. Volume is fitted via a least squares technique to the Murnaghad equation.

Materials can and do behave asymmetrically with respect to applied stresses vectors (i.e. applying stress to a unit cell in a particular vector will distort the cell a different amount as compared to stress vector in a different vector). This asymmetric response is due to the crystal structure of materials. Calculations were carefully analyzed in the Energy vs. Volume curves to ensure this does not happen by only modulating the volume of the whole cell in fixed steps.

Heat of formation (H^f) was calculated using the following formulation[27, 28, 33]

$$H^f(\mu_{Ta}, \mu_N) \approx \frac{E_{TaN}^{Cell} - n\mu_{Ta} - m\mu_N}{m+n}$$
$$\mu_N = 0.5E_{N_2}^{total} \qquad (9)$$
$$\mu_{Ta} = E_{Ta-Bulk}^{total}$$

The E^{Cell}_{TaN}, E^{total}_{N2}, and $E^{total}_{Ta\text{-}Bulk}$ are the enthalpies of TaN (bulk), N_2 (gas) and Ta (BCC), respectively and n are the number of Tantalums in the unit cell and m is the number of nitrogens in the unit cell. Reference chemical potential states for Ta and N were considered to be Ta-BCC and N_2 (gas), and were also calculated using VASP. Ta-BCC had a k-space of 11x11x11 with Monkhourst Pack with a planewave cut off of 400eV and a_0 was 3.30 Ang with convergence to < 1 meV/at and found to have chemical potential of -11.8653 eV/at. Chemical potential for N_2 was calculated in a large supercell box of 20x20x20 Angstroms, 1x1x1 k point with a planewave cutoff of 400 eV and found to be -8.2996 eV/at with a bond length of 1.109 Ang.

The cohesive energy is the energy needed to dissociate the material into isolated atoms. [50]

$$E_C = \frac{H_{Cell} - \sum_{i=1...N} iH_i}{\sum_{i=1...N} i} \qquad 10$$

Where E_c is the Cohesive Energy, H_{cell} is the ground state energy of the unit cell. H_i is the energy for the individual, isolated atoms of the system. The cohesive energy gives the difference between the ground state of chemical materials to the energy of the isolated species and provides a measure of the energy needed to dissociate the system. This would be an important metric where vacuum based depositions are involved such as PVD or CVD. Cohesive energy and heat of formation provide similar information on phase stability, but with different reference states.

The Density of States (DOS), Charge Density Plot and Electron Localized Functional (ELF) were determined and analyzed for both the NaCl and hexagonal phases (CoSn and Fe_2P) with the k-space increased to 21x21x21 and 21x21x19, respectively. The DOS for all systems was shifted so the Fermi-energy was zero. The charge density and ELF plots were qualitatively analyzed with the Visual Molecular Dynamics (VMD, version 1.8.7) program.[61] To quantify charge and ionic radii, a Bader analysis was completed on the system with the Fourier transform grid increased significantly. The NaCl had a 210x210x210 mesh, the CoSn had a 224x224x125 mesh, and the Fe_2P had a 240x240x140 mesh. All calculations used a GGE-PBE exchange correlation functional. The analysis was based off the fast algorithm described by Tang.[65]

Lattice Calculations

Table 7 has results of the lattice parameters for all three phases along with published experimental values (at room temperature) and *ab initio* studies in the

literature. In general there is good agreement between the current calculations and experimental data and previous calculations. All the lattice constants determined in this study are within the published range of *ab initio* studies done in prior art. NaCl shows an increase in a_0 from LDA to GGA-PW91 to GGA-PBE. CoSn shows a smaller change, but the same trend for a_0. For c_0, the order is changed slightly with order from smallest to largest being LDA to GGA-PBE to GGA-PW91. The Fe_2P phase has the LDA being slightly smaller when compared to the GGA-PBE and GGA-PW91, but the GGA are fairly close together with only the c_0 showing a difference between the two potentials. In addition, the Fe2P and the CoSn lattice constants are close to each other and to the experimental values for CoSn. LDA typically over estimates the enthalpy and thus underestimates the lattice constants, whereas GGA-PW91 and GGA-PBE do the inverse, and that is what is observed.[43, 51]

Table 7. Results for the lattice parameters, previously published studies and experimental results found in the literature. All Values in Angstroms.*All experimental values are at Room Temperature.

		NaCl	CoSn		Fe_2P	
		a_0	a_0	c_0	a_0	c_0
LDA	Study	4.353	5.17	2.92	5.15	2.87
	Lit	4.235($TaN_{1.3}$)[29] 4.2928 ($TaN_{1.1}$)[29] 4.326[69] 4.33[70] 4.357[29]	5.1546[29]	2.8906[29]		
GGA-PW91	Study	4.3978	5.22	2.94	5.22	2.91
GGA-PBE	Study	4.424	5.27	2.93	5.22	2.92
	Lit	4.395[28] 4.406[32] 4.413[25] 4.414[26] 4.414[36] 4.415[33] 4.42[70]	5.221[25] 5.238[32] 5.297[33]	2.921[25] 2.913[32] 3.175[33]	5.226[26,] 5.229[36]	2.92[26,] 2.918[36]
Experiment*		4.35[24]			5.186[35]	2.91[35]

The Energy vs. Volume curve (Figure 8) suggests that the Fe_2P phase is the preferred thermodynamic crystal structure of the three, by ~ 0.3 eV/at, with the order of the stability being Fe2P > NaCl > CoSn.. This relative stability is consistent for all three exchange-correlation functionals. This calculation is consistent with the phase diagram, as the NaCl phase does not occur until high temperature. Figure 8 shows the PBE calculations; the results are similar for LDA and GGA-PW91. .

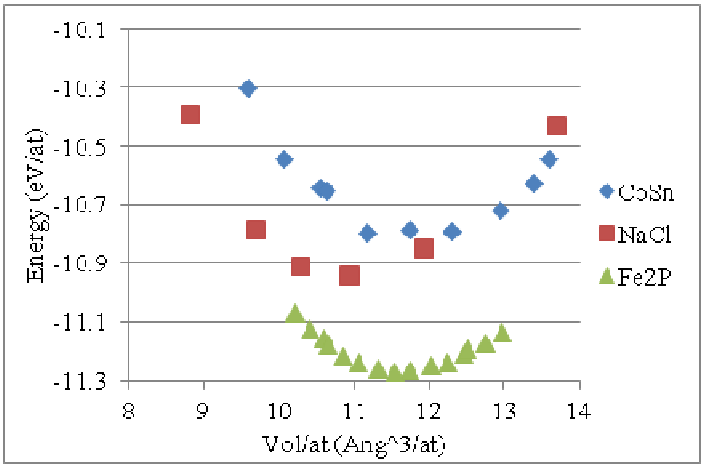

Figure 8. Calculated energy vs volume curves for the NaCl, CoSn and Fe_2P phases of Tantalum Nitride

Bulk Studies - Modulus

The bulk modulus calculations are shown in Table 8 alongside the experimental values for bulk modulus. The experimental data is taken at room temperature and it should be noted that there should be a small increase in the modulus at zero Kelvin.[67] For example, Silicon Nitride (Si_3N_4) experiences a 2% increase when going from room temperature to 30 K.[68]

In general there is reasonable agreement between the present results and experimental measurements and previous calculations. For all three methods (LDA, GGA-PW91, GGA-PBE) the results are in close agreement with experiment for the Fe_2P phase (when the measurement was done, it was believed to have been for the CoSn

phase, but it was likely to actually have been for the Fe_2P phase). For the CoSn phase, the comparison of the present calculations with experiment is slightly worse for the LDA and GGA-PW91, but this is likely due to the experimental value being for the Fe_2P phase, not the CoSn phase. For the NaCl phase, the three methods are in reasonable agreement with the experimental value, with the LDA having a slightly lower value, and the GGA-PBE having a slightly higher value.

Thermodynamic Properties Results and Discussion

For Cohesive Energy, the order of stability is Fe2P>CoSn>NaCl with the difference between the phases being 0.2 to 0.06 eV/at for all exchange correlation functions studied as shown in Table 9. The only published value found for the cohesive energy is derived from a different calculation than what was used here as Cao used the fitted energy minimum from the bulk modulus calculation as the cohesive energy value.[25]

The Heat of Formation calculation suggests a similar result as the Cohesive Energy, where the CoSn phase is metastable when compared to the NaCl phase. For both Cohesive Energy and Heat of Formation, Fe_2P is the lowest.

Table 8. *Ab initio* results for Bulk Modulus (GPa) for the 3 phases, experimentally found results and published ab initio values. *Experiments are at Room Temperature. ** The value listed is for a phase which was believed to be CoSn, but could have been Fe_2P.

		NaCl	CoSn	Fe_2P
LDA	Study	341.74	280.78	327.87
	Lit	379.6[69] 403.85[70]		
GGA-PW91	Study	297.79	268.32	333.61
GGA-PBE	Study	394.57	317.87	322.09
	Lit	327.6[25] 328.3[70] 347[33] 349[36] 375[28]	251[33] 303.6[25]	320[36] 319[33]
Experiment*		349*[71]		320 ± 11[71]**

Table 9. Calculated Cohesive Energy for NaCl, CoSn and Fe_2P phases

	NaCl	CoSn	Fe_2P
LDA	-10.71	-10.53	-10.96
GGA-PW91	-9.6	-9.46	-9.83
GGA-PBE	-9.45	-9.39	-9.78
Ab Initio Studies	-13.38[25]	-14.05 [25]	

The results for Heat of Formation are listed in Table 10 for all phases and include experimental and theoretical literature values. For the present calculations, all three methods (LDA, GGA-PW91, and GGA-PBE) find that the heat of formation is largest for the Fe_2P phase, suggesting that it is the most stable. The calculated values for the Fe_2P phase are in good agreement with the experimental value, which was believed to be for a CoSn phase, but likely could have been the Fe_2P phase. There is no experimental value for the NaCl phase for comparison, but since it is less stable at low temperatures it must have a lower heat of formation, consistent with the present calculation. All three methods find that the heat of formation is slightly larger in magnitude for the NaCl phase compared to the CoSn phase, in agreement with previous calculations for heat of formation, and contradicts the Cohesive Energy results of Cao.[25]

Fe_2P appears to be the more stable phase when compared to CoSn. The location of the Tantalums is the same between the two crystal structures. The change in the distance and a symmetric distribution of the Nitrogens in the Fe_2P structure is the difference. For the two crystal structures, it can be seen that there are two types of Tantalums as shown in figure 9 and labeled to highlight the two types of Tantalums in the two crystal structures. The redistribution of the Nitrogens is the reason for the stronger bonding occurring through the Fe_2P structure. In addition, the difference in the Tantalum bonding should be obvious in the bond and electric characterization.

Table 10. *Ab initio* and experimental results for Heat of Formation (eV/atom) for the 3 phases. *Experiments are at Room Temperature, and the value listed is for a phase which was believed to be CoSn, but was probably Fe_2P. ** Values were calculated based on functional units of TaN and not atom based.

		NaCl	CoSn	Fe_2P
LDA	study	-1.33	-1.15	-1.58
	Lit	-1.29[29] -1.305[27,] -1.39 ($TaN_{1.1}$)[29] -1.4 ($TaN_{1.3}$)[29]	-1.117[27,] -1.11[29]	
GGA-PW91	Study	-0.98	-0.856	-1.22
GGA-PBE	Study	-0.872	-0.809	-1.20
	Lit	-0.86[33,] -0.875[26] -0.976[28] -1[32]	0.11[33,] -0.745[26] -0.86[32]	-1.185[33] -1.195[26]
Experiment			-1.3[72]	

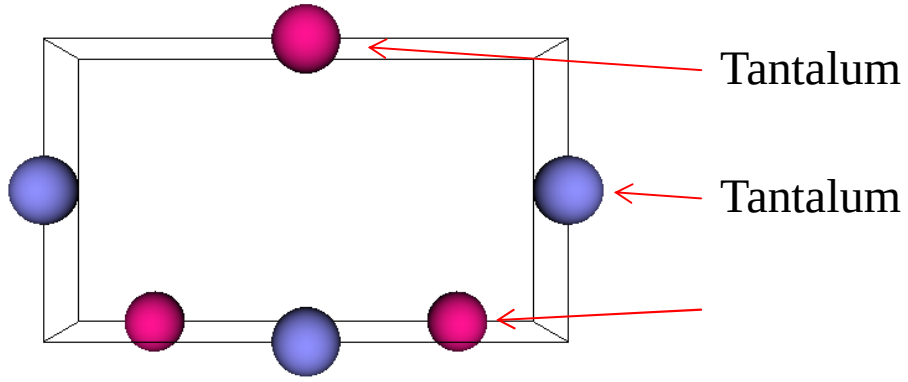

Figure 9. Location of different types of Tantalums compared to Nitrogen in the CoSn and Fe_2P phases based on Basis set.

Density of States, Electron Localization Functional and Bader Analysis

The Density of States (DOS) are shown in Figure 10. Based on the DOS, NaCl, Fe_2P and CoSn are metallic and are comparable to other ab initio studies.[25, 26, 36] The large number of states in the -10 to -3 eV region suggest a significant amount of covalent bonding occurring between the N2p and the Ta5d. As there are 2 types of tantalums in the Fe_2P and CoSn phases, both are shown and the DOS shows significant differences in the DOS of the Tantalums in the CoSn's and the Ta-2 atom having greater bonding than

the Ta-1 atom. The Fe2P phase suggests that this bonding difference is less when comparing the Ta-1 to Ta-2 DOS's. The NaCl DOS suggest a significant amount of states at the Fermi level which is dominated by the Ta5d orbitals.

The Charge Density and Electron localization functional were plotted and analyzed and shown in Figure 11, 12, and 13. The ELF and Charge density plots indicate the NaCl-TaN bonding is ionic with charge residing on the nitrogen as there are no other electrons associated with the other ionic species. The CoSn-TaN charge density shows the bonding to be occurring between the Ta-2 and the Nitrogen. The ELF suggests the bonding occurring between the Nitrogen and Ta-2 is metallic to ionic. The Fe_2P charge density of this system suggests there is bonding occurring similarly for the Tantalum's to the Nitrogen's.

The Bader analysis results are shown in Table 11. For CoSn and Fe_2P, Tantalum 1 is located on (0001) and Tantalum 2&3 are located on (0002). The charge on each of the atoms is based on taking the difference of the valence electrons as defined by the PAW's and subtracting the number of electrons as determined by the analysis. Tantalum has 11 valence electrons and Nitrogen has 5 valence electrons. For all three structures there is a large transfer of charge from the Ta to the N, but for the CoSn and Fe_2P structures there is a difference between the two Tantalum sites, with the CoSn having a larger difference between the two Ta sites (1.4 electrons) than in the Fe_2P structure (0.6 electrons). The radii and Bader Volume follow a similar trend where the Tantalums have a larger difference in the CoSn phase compared to the Fe_2P. N has a larger radius in the NaCl phase than in the other two phases. However, the Bader Analysis, ELF, and volume vs. energy curves support Fe_2P as the more stable phase

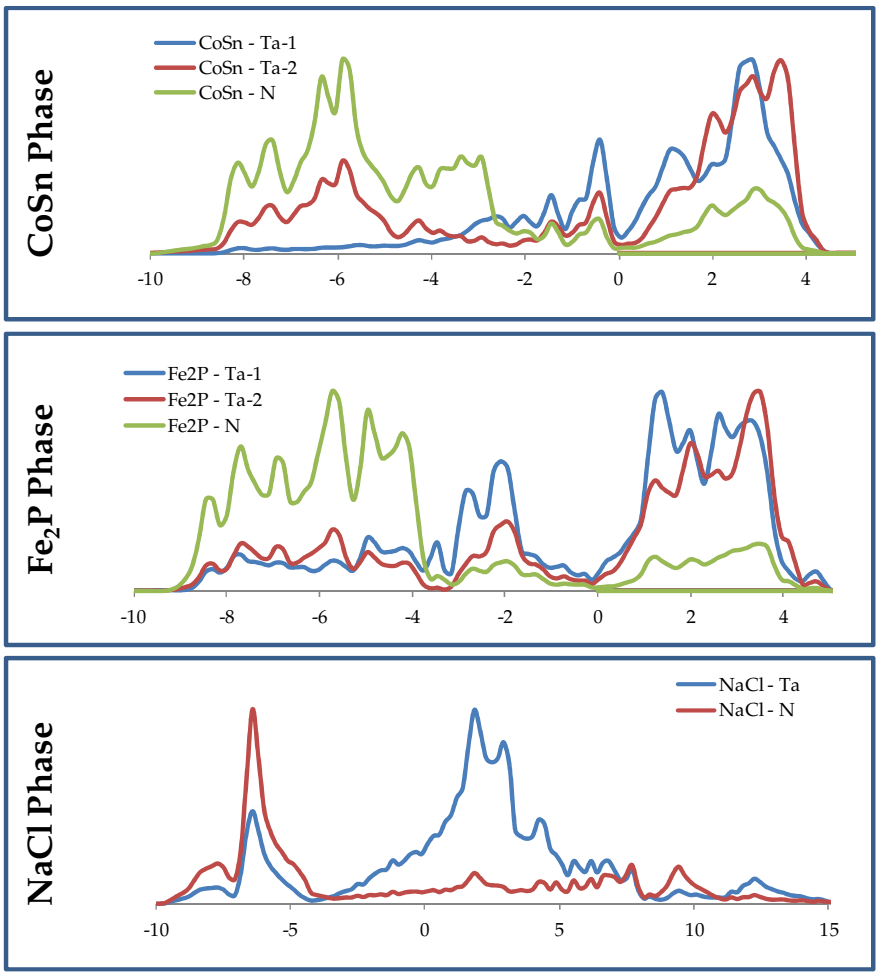

Figure 10. Density of States of Tantalum Nitride. The three phases appear metallic. Fermi Energy for all three phases is shifted to 0 eV.

The percent ionicity was calculated based on Equation 11 as shown below.

$$\%\ Ionicity = 1 - e^{-0.25*|Electronegativity\ difference|^2} \qquad 11$$

Nitrogen and Tantalum have an Allen Electronegative of 3.066 and 1.34, respectively. [20] This means the % ionicity of a Ta-N bond is 53%. The structure should exhibit more covalent bonding than an ionic bonding. The calculation ignores the fact that there are two types of Tantalums in the system.

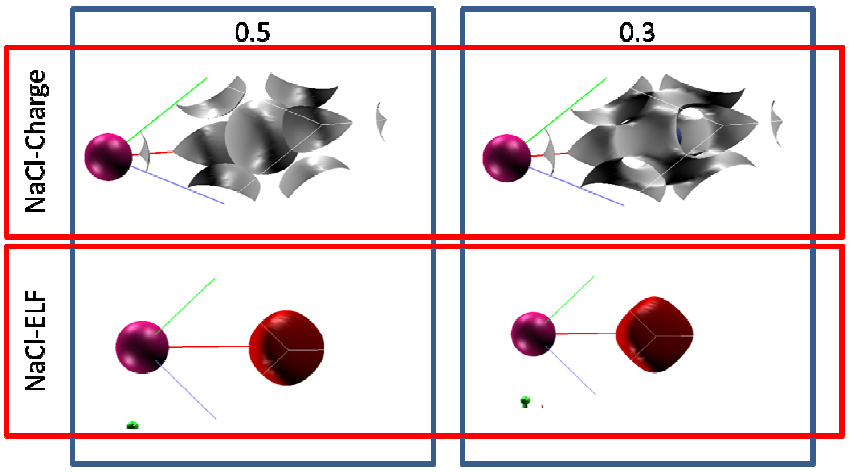

Figure 11. Iso-contours for the Charge Density and Electron Localization Functional for NaCl-TaN.

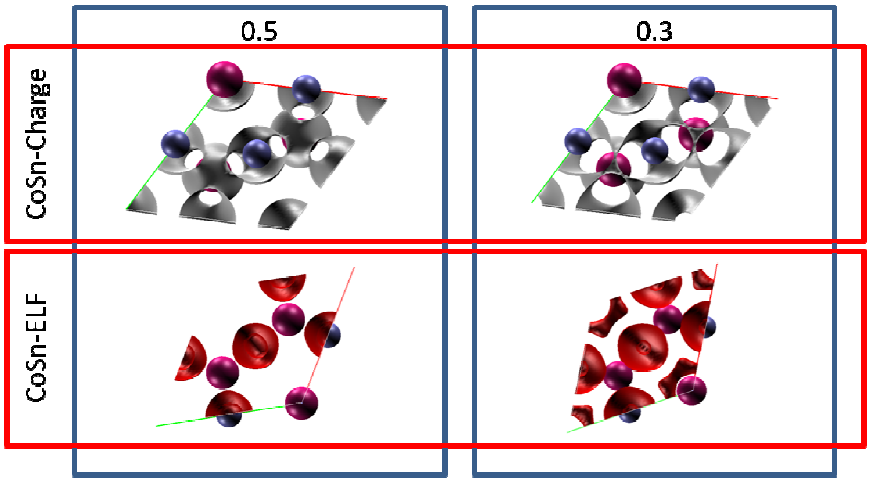

Figure 12. Iso-contours for the Charge Density and Electron Localization Functional for CoSn-TaN.

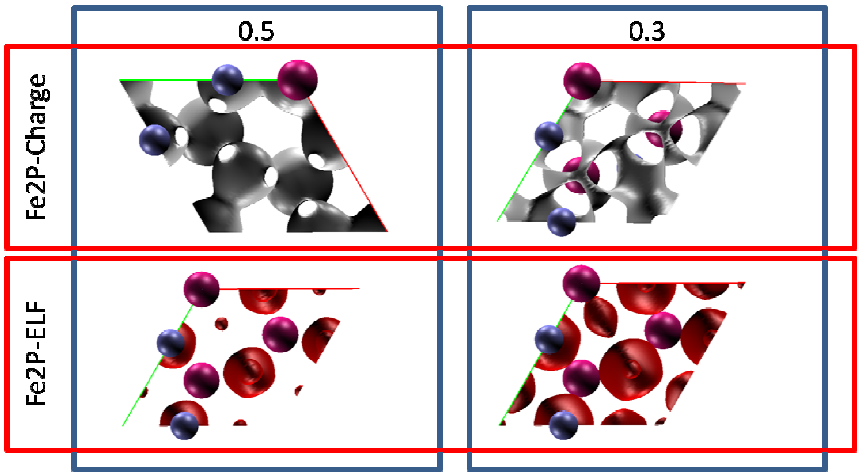

Figure 13. Iso-contours for the Charge Density and Electron Localization Functional for Fe_2P-TaN.

Table 11. Bader Analysis Results for all 3 phases.

			NaCl	CoSn	Fe_2P
Valence Electrons	Tantalum	1	9.06	10.20	9.67
		2 &3		8.77	9.04
	Nitrogen		6.94	6.75	6.75
Charge	Tantalum	1	1.94	0.80	1.33
		2 &3		2.23	1.96
	Nitrogen		-1.94	-1.75	-1.75
Bader volume (Ang^3)	Tantalum	1	11.56	17.95	14.85
		2 &3		10.39	11.44
	Nitrogen		11.45	10.58	10.48
Radius (Ang)	Tantalum	1	1.12	1.28	1.03
		2 &3		1.04	1.07
	Nitrogen		1.11	0.99	0.97

Summary

The existence of the Fe_2P phase for TaN has been noted in experimental work and *ab initio* work has proposed this phase over the CoSn phase. [26, 33, 36] All three exchange-functionals result in the same relative order of stability, Fe2P>CoSn>NaCl. This is consistent with one study by Zhao who investigated all three structures using one exchange-correlation functional PBE-GGA and consistent with two other *ab initio* studies finding CoSn metastable when compared to either Fe_2P or NaCl.[27, 28] The stability of the phase has been shown over three different exchange correlation functionals.

The bulk studies show good agreement with experimental lattice constants for all three phases. The Bulk modulus for the Fe_2P phase show reasonable agreement across all of the methods and appear close to the experimental Bulk modulus reported for the CoSn phase, but probably was the Fe2P phase. The Fe_2P phase has the lowest Heat of Formation energy across all methods. In addition, the Bader Analysis finds that the two Ta sites in the the Fe_2P phase have more similar charge than in the CoSn structure. The Bader Analysis is qualitatively supported by the ELF study. Figure 9 also shows the

different Tantalum's determined by the ELF, Charge Density Plots and Bader Analysis. It would be expected that these different Tantalums would have different vacancy formation enthalpies and that the (0001) and (0002) surfaces should be different in energy.

For the next chapter, we will focus on just one functional, to reduce computational cost and since the three funcationals give very similar results. We choose the GGA-PBE, since it yields slightly better comparison with experiment First, looking at the lattice constants and bulk modulus, the GGA-PBE comes very close to the experimental value for the CoSn and Fe_2P phases. Second, the focus of the surface studies is on the CoSn and Fe_2P phases as these are unexplored and one of the crystal structures is the ambient system. It should be noted, if the author was interested in the surface of NaCl-TaN, a different conclusion is reached and the LDA exchange correlation function would be used.

Chapter 5

POINT DEFECTS IN BULK TANTALUM NITRIDE

Crystal materials have point defects which result in different physical phenomenal possible, such as diffusion and atomic re-arrangement to other crystal structures. The defects in a material can significantly alter the macroscopic properties. Examples of this are semiconductor doping and electrical properties, dislocation glide and yield strength of materials. There are several types of point defects including interstitials, vacancies, and anti-site defects. This work is focused on point defects of the CoSn, Fe_2P and NaCl phases. There are 3 types of vacancies in the hexagonal crystal structures as can be seen in the basis of the crystal and in Figure 14. The NaCl phase forms a eutectic with the Fe_2P and the Ta_2N as can be seen in the phase diagram. The vacancy formation energy is a very important factor in determining the composition range of ordered compounds like NaCl, CoSn, and Fe2P, and will be investigated in this chapter.

Defect Analysis Methods

Point defect stability in tantalum nitride will be assessed for CoSn-TaN. The vacancy formation energy (E_f) is defined as the energy needed to form a vacancy and is calculated as follows[32]

$$E_f = \left(E_{n-1} - \frac{n-1}{n} E_n \right) \qquad 12$$

Where E_n is the energy of the system without a vacancy, n is the number of atoms in the system, and E_{n-1} is the energy of the system with a vacancy.

As TaN is a binary compound, the Energy of Formation for the defect is then related to the chemical species that is

$$E_f^X = E_{Vacc,n-1}^X - E_n + \mu^X \qquad 13$$

Where the Energy of Formation with respect to the specific vacancy species is defined by the energy as calculated with atomic species missing, in this case Tantalum or Nitrogen. E_n is the calculated energy of the system with no vacancy, and μ is the chemical potential of the species removed from the system.

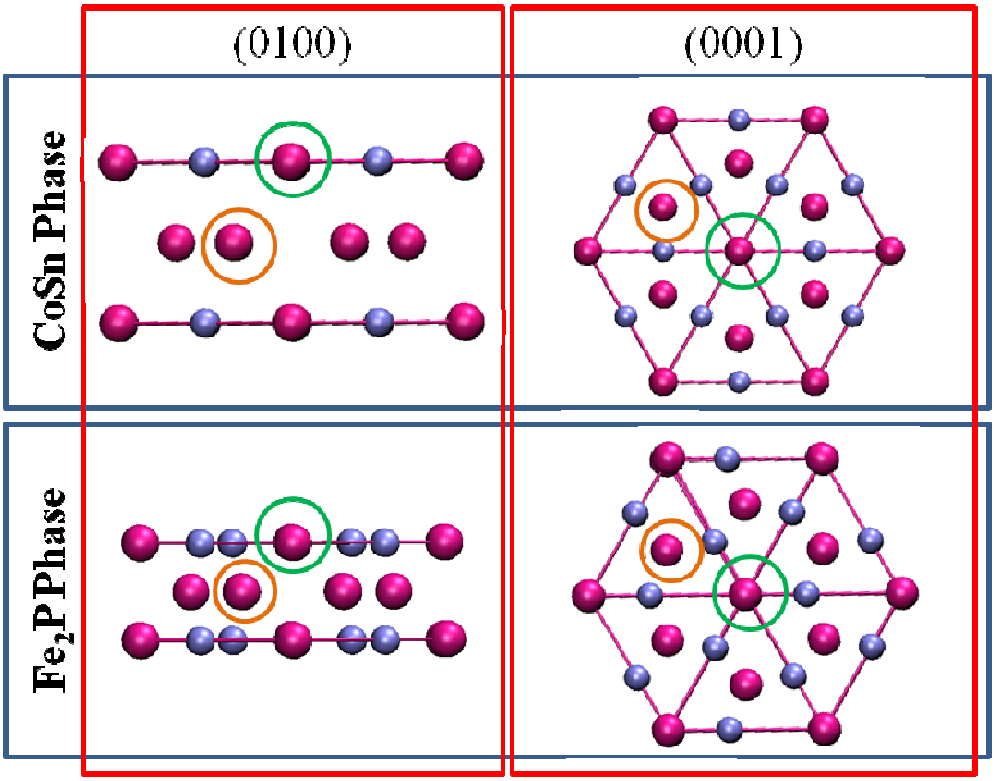

Figure 14. Crystal structures for CoSn and Fe2P TaN. The Nitrogens ( ) and Tantalums ( ) shifts can be seen in and are slight between the two phases. The Two types of vacancies are highlighted in the diagrams. Tantalum Vacancy location 1 is circled in Green and Tantalum Vacancy location 2 is circled in Orange.

The chemical potentials of the system are constrained by looking at the systems energy and comparing the summation of the chemical potentials of the systems defined by the following in a binary system

$$E_n = x\mu^{Ta} + y\mu^N \qquad 14$$

Where μ^X is the chemical potential for chemical species X (Ta or N) and x, y are the number of species in the compound. In addition, the chemical potential could be looked up in various thermodynamic tables or calculated from first principles.

For calculations involving more than 1 vacancy, the equation becomes

$$E_f^X = \frac{E_{Vacc,n-m}^X - E_n + m\mu^X}{m} \quad 15$$

Where the equation is the same as the single vacancy formation energy except it is corrected for m number of vacancies. The calculation is done only with the NaCl-TaN phase as it is the only one that suggests it is stable off stoichiometry.

The crystals were 96 atom systems, GGA-PBE exchange correlation functional and planewave cutoff at 520 eV was used as the crystal system will have a vacancy in it and the planewave needs to be expanded enough to ensure convergence in the vacancy location as advised in the VASP manual. A 5x5x3 K space with Gamma centering was also used. A conjugant gradient method was used for the relaxation of the system with 8 ionic steps at a minimum and converged to < 1 meV/at.

CoSn-TaN Vacancies

In this study, the vacancies have positive formation energy as shown in Table 12 indicating vacancies are enthalpically unfavorable as expected. Table 13 summarizes the atomic movements during relaxation. The Ta vacancies have a higher formation energy associated with them compared to the Nitrogen vacancy. The nearest neighbor movements are shown for the surrounding lattice, atomic movements of all 3 defect types in Figure 15.

The Nitrogen vacancy (V_N) has a reduction in the supercell volume with a reduction in the (0001) area, but an increase in the [0001]. The V_N shows a large

displacement of the surrounding nitrogen atoms around the defect center as shown in figure15. The tantalum atoms nearest neighbors show little movement relative to the nitrogen atom. The nitrogen atoms are drawn toward the defect center and show a symmetric response around the defect center. The Nitrogen is slightly smaller than either of the Tantalums and therefor would move slightly easier than either.

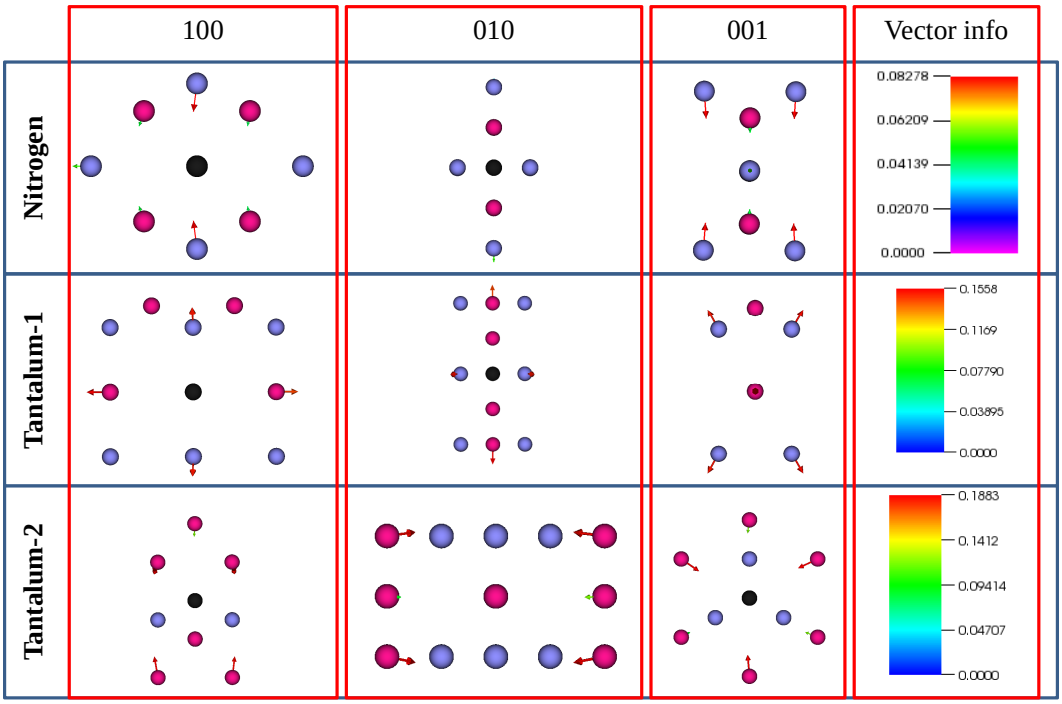

Figure 15. CoSn-TaN Nearest Neighbor movements around vacancies. The Nitrogens ( ) Tantalums ( ) , and Vacanies ( ) are shown.

The Tantalum-1 vacancy (V_{Ta-1}) type defect resulted in little change in length in the (0001), but a small increase in [0001], which results in a small, net increase in the crystal volume. The V_{Ta-1} defect results in a symmetric movement of the Ta and N nearest neighbors away from the defect center as shown in Figure 15. The N atoms in the same (0001) as the V_{Ta-1} defect symmetrically moves away from the defect center at the same magnitude. The Tantalum atoms on the [0001] direction above and below the V_{Ta-1} move away from the defect center. This system repulsion seems to allow for little

reduction in the overall super lattice size and would result in a large vacancy in the center of the crystal that could allow for easy movement of other defect types. The ELF and Bader Analysis suggest that the Ta-1 location is less bound than the Ta-2 location to the N as noted in Chapter 4.

Table 12. The enthalpy of formation for vacancy formation energies in the crystal phases studied. NaCl has 64 and 63 atom cells for perfect and defect systems, respectively. The hexagonal phases have 96 and 95 atoms for the perfect and defect crystals, respectively

Phase	Cell	Formation Energy (eV)	Crystal Vectors (Ang)			Cell Vol (Ang^3)	Vol Change (Ang^3)	%Vol Change
			x	y	z			
NaCl	Base		8.85			692.24		
	V_N	0.108	8.84			690.82	1.42	-0.2%
	V_{Ta}	-1.508	8.82			685.73	6.51	-0.9%
CoSn	Base		10.54	10.54	11.71	1126.05		
	V_N	1.28	10.49	10.49	11.73	1120.96	-5.1	-0.45%
	V_{Ta-1}	1.00	10.54	10.54	11.72	1126.40	0.4	0.03%
	V_{Ta-2}	2.57	10.51	10.51	11.72	1120.32	-5.7	-0.51%
Fe_2P	Base		10.47	10.47	11.7	1110.51		
	V_N	3.07	10.45	10.45	11.72	1108.30	-2.2	-0.20%
	V_{Ta-1}	3.48	10.47	10.47	11.67	1107.14	-3.4	-0.30%
	V_{Ta-2}	2.51	10.46	10.46	11.68	1107.03	-3.5	-0.31%

The Tantalum-2 Vacancy (V_{Ta-2}) shows a reduction in the supercell volume with a reduction in the (0001) area, but an increase in the [0001] dimension. The V_{Ta-2} defect shows movement of nearest neighbor Ta atoms towards the defect center with the nitrogen moving very little as shown in Figure 15. The difference in the V_{Ta-1} and V_{Ta-2} defects suggest a potential preferred path for vacancy diffusion and substitutional diffusion. The V_{Ta-2} defect shows a greater release of energy upon relaxation than all of the studied defects. This is consistent with the ELF and Bader Analysis results as these two types of Tantalum sites have different bonding natures in the crystal as Ta-2 has the largest positive charge on it.

Table 13. Assessment of supercell distortions for Vacancy defects and perfect cells. NN is Nearest Neighbor for CoSn vacancies largest absolute move is relative to perfect crystal position.

Vacancy type	Largest atomic movement	Largest atomic movement species	Position	Largest absolute movement (Ang)	Total species moving max
V_N	Towards defect center	Nitrogen	2nd NN	0.083	4
	Away from defect center	Nitrogen	NN	0.156	6
V_{Ta-1}	Away from defect center	Tantalum	Mirror Ta	0.156	2
V_{Ta-2}	Towards Defect center	Tantalum	2nd NN	0.188	6

Fe_2P-TaN Vacancies

The convention of naming the vacancies was maintained from the CoSn phase. The defect energies are all larger than the CoSn phase defects, which means they are less favored to form energetically compared to the CoSn phase defects. The defect studies were repeated with a slight increase in the crystal lattice dimension to ensure the values reportedly converged the same and there was limited numerical noise in the calculation. It should be noted that the crystal lattice did not change much with the volume decreasing by 0.2% to 0.3% for all 3 vacancies. The tantalum vacancies showed a larger decrease compared to the Nitrogen vacancy volume decrease. The majority of the volume change is associated with a compression in the Z axis for the tantalums and the nitrogen showed ~ 0.2% reductions in all directions.

The nearest neighbors of the defects in the Fe_2P supercell, showed no movement. The Tantalum in the (0001) shows similar energy released compared to the nitrogen, but greater than the energy associated with the other Tantalum vacancy. The Bader analysis suggests that the Tantalum is larger compared to the other tantalum and thus would leave a larger vacancy in the system. A V_{Ta-2} should be more stable as it would create less of a

volume change. This would be balanced by the fact that the Ta-2 has a different number of bonds to the Nitrogens when compared to the Ta-1. The Ta-2 should leave greater number of dangling bonds associated with the surrounding Nitrogens. Comparing the Bader analysis results to the defect formation energies calculated show similar trends. The Vacancy Energy of the CoSn phase show wide variance between the two sites compared to the Fe2P, similar to larger variations in the ionic charge. The V_{Ta-2} defect is lower in formation energy than the V_N or V_{Ta-1} defects. The Bader analysis suggests that the Nitrogen and Tantalum-1 have less of an absolute charge when compared to the Tantalum-2 species.

NaCl-TaN Vacancies

The NaCl phase has small, but positive formation energy for the Nitrogen vacancy. The Tantalum vacancy in the NaCl phase shows a relatively large, negative enthalpy for formation, so formation is very favorable. This was studied further by removing additional Tantalums for the 64 atom cell. Supercells with Two and 8 Vacancies were created, corresponding to compositions of 48% and 43% N, respectively. The two vacancy cell involves placing the two vacancies fare from one another. The 8 Vacancy cell was evenly distributed in the 64 atom cell by using the fact that the cell is made up of 8 smaller cells. Since the vacancies are charged, it is likely that they would distribute evenly to maximize their separation. The 8 vacancy cell corresponds to a 43 at % which is the eutectoid point for the NaCl structure. . The results of the additional vacancies are plotted in Figure 16 and the Enthalpies are provided in Table 14. Since the NaCl phase forms at high temperatures, entropy effects are significant, so the ideal Entropy of mixing was added to each of the cells by a calculation of the configurational entropy using Boltzmann's Entropy formula: [73]

$$S = k_b Ln\left(\frac{N!}{\prod_i N_i!}\right) \quad 16$$

Where S is the entropy k_B is Boltzmann's Constant, N is the total number of sites in the cell. N_i is the number of sites either occupied by Tantalum or Nitrogen. The entropy is then input into a Gibb's Free energy calculation with G = H –ST where H is the enthalpy and T is the temperature. The analysis was done at the eutectoid temperature (T = 1993 K) from the phase diagram. The Figure 17 shows Enthalpy and the Configurational Entropy. The result is a drop in the Gibbs energy for the Tantalum nitride curve. The shift in of the Enthalpy+Entropy curve would be more if one adds in the vibrational entropy component (not calculated), and would shift the eutectoid point towards a lower composition, and would increase agreement with experiment. .

Overall, the results show that vacancy formation is favorable in the NaCl structure. The difference in Gibb's free energy is small across a wide composition range, from 43% to 50%, consistent with the experimental phase diagram which shows that the NaCl phase forms from 42 at% to 50 at%..

Nitrogen vacancy has a small volume change. The Tantalum vacancy has a large change volume and largest of the studied vacancies. For the Nearest Neighbors (NN) for V_N in the NaCl phase moved inward by 6% and for the V_{Ta} vacancy, NN moved inward by 2%. This is comparable to other studies which found a 7 to 10% and 3 % in ward movement for the V_N and V_{Ta}, respectively.

Summary

The enthalpy of vacancy formation shows the Fe_2P phase to have larger energies for ions to be removed compared to the CoSn phase, which is consistent with the Fe2P phase being more stable. The high vacancy formation energy on the Ta and N sites

suggests that Fe2P would exist as a line compound, which is what is observed on the experimental phase diagram. In contrast, in the NaCl structure, vacancy formation on the Ta sites is favorable, with only small differences in Gibb's free energy from 43% to 50% N, which is consistent with the experimental phase diagram showing that the NaCl structure forms from 42 at% to 50 at%.

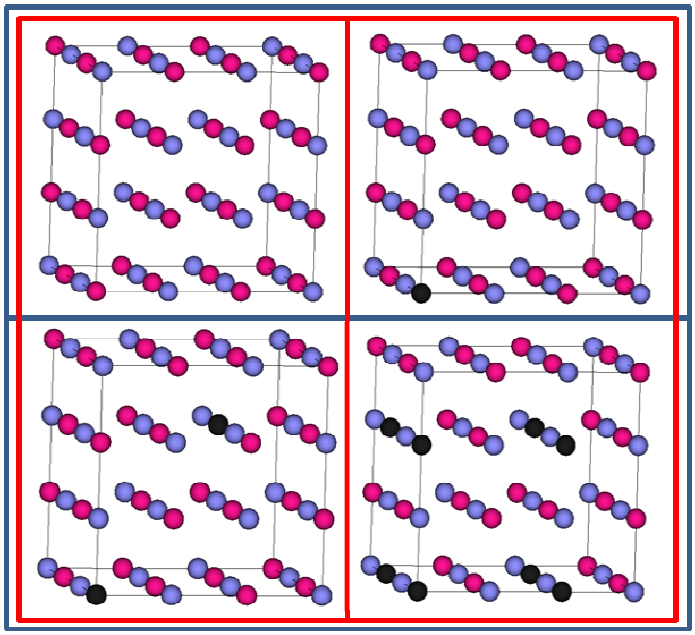

Figure 16. NaCl-TaN 64 atom supercell showing location of vacancies. Upper left is the perfect crystal. Upper right has a single Tantalum Vacancy. Lower left has 2 Tantalum Vacancies. Lower Right has 8 Tantalum Vacancies placed by repeating an 8 atom lattice. The Nitrogen ( ) Tantalums ( ) , and Vacancies ( ) are shown.

Table 14. Table of the Enthalpy for additional vacancies in at 64 atom supercell of NaCl-TaN.

Cell	Enthalpy (eV/at)	a_0 (Ang)	Cell Vol (Ang^3)	Vol Change (Ang^3)	%Vol Change
Perfect	-10.94	4.424	692.24		
V_N	-10.98	4.42	690.82	1.42	-0.2%
V_{Ta}	-10.95	4.41	685.73	6.51	-0.9%
$2V_{Ta}$	-10.97	4.40	679.87	12.37	-1.8%
$8V_{Ta}$	-10.82	4.30	637.41	54.83	-7.9%

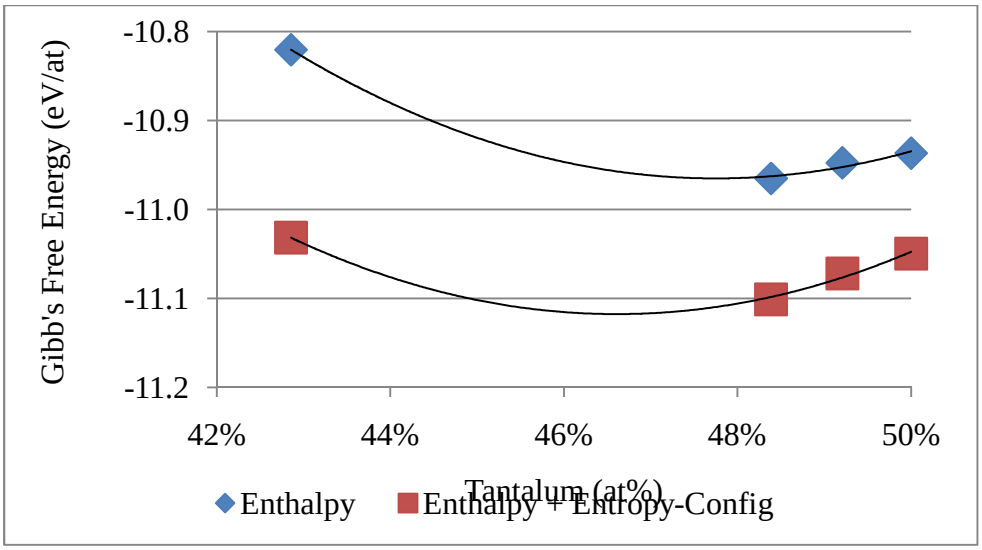

Figure 17. Graph of the Enthalpy and Gibbs Free Energy at1993K (Enthalpy + Entropy-Config) curve for varied atomic compositions of the NaCl-TaN phase.

Chapter 6

TANTALUM NITRIDE SURFCE AND ADATOMS

As the metal interconnects can be formed by atomic deposition techniques, adatoms begin the early stages of nucleation and interface formation. At the surface, diffusion, re-arrangement and interlattice changes attempt to lower the systems energy. Atomic deposition techniques are constrained by these physical phenomena from a thermodynamic perspective. A key to this is the understanding of the TaN surface and Adatom adhesion. Adatoms drive the way interfaces may form as they provide insight into how two different elements may interact at an interface.

This chapter first calculates bonding energy between isolated (gas phase) single atoms of Tantalums and Nitrogens to a single Silver atom. Then the surface energy of 2 close packed surfaces of Fe_2P-TaN are calculated and assessed as a function of partial pressure of Nitrogen to understand which surface will be stable in a vacuum environment. Next a study of the absorption enthalpies for Silver adatoms will be done to understand which sites are preferred for adsorption, including single atoms, two adatoms, and a sub-monolayer. Finally, a calculation of the thin 4-layer slab of silver on a Tantalum Nitride surface will be calculated to understand the interface of Tantalum Nitride and Silver thin films.

Bond Energy calculations

A single atom of Silver was placed in a large supercell with either a Tantalum or Nitrogen. The molecule was allowed to relax. The k-space is set at 1x1x1 according to the standard method to assess isolated atoms or isolated molecules. The exchange correlation functional used was the GGA-PBE. The planewave cutoff and cell size were increased to ensure convergence which was determined to be < 1 meV/at. Figure 18

shows the results of the convergence which was very stable across the calculations. The Bond energy was determined by the following equation

$$E_{Bond} = E_{Ag+Ta\ or\ N} - E_{Ta\ or\ N} - E_{Ag} \qquad 17$$

Where the Bond Energy and Calculated Energy are E_{Bond}, and $E_{Ag+\ Ta\ or\ N}$, respectively. The isolated atoms, $E_{Ta\ or\ N}$ and E_{Ag}, are the same values as used in the Cohesive Energy calculations of Chapter 4. The Tantalum-Silver bond energy was determined to be -2.93 eV and the Nitrogen-Silver bond energy was found to be -4.47 eV at a planewave cutoff of 520 eV. This is a theoretical value for a bond between the two elements and provides insight into which bonding sites may be preferred on the surface of the Tantalum Nitride. In this case, it suggests that the silver will prefer to bond to nitrogen, not tantalum. This will be taken into consideration when looking at bonding sites for surface absorption studies.

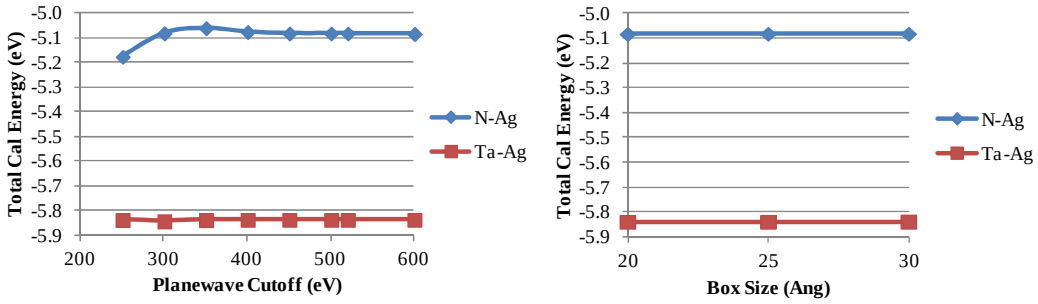

Figure 18. Energy convergence for bond energy calculations for Nitrogen-Silver and Tantalum-Silver.

Surface Energy Calculations

This study looks at the stability of the close packed layers of the Fe_2P to determine which surface is thermodynamically more stable. There are 2 surfaces that were analyzed in this study, the (0001) and the (0002). The (0001) is a mixed Nitrogen

and Tantalum surface which has a ratio of 2:1 and is Nitrogen rich. The (0002) surface is only Tantalum. The method to calculate this was to use 2 different slabs which were not stoichiometric and correct for the differences as noted in the surface section.

Surfaces can have reconstruction and/or relaxation. Surface relaxation involves the inter-plane distances contracting or expanding to help compensate for the additional energy associated with the exposed surface. Surface relaxation occurs in the plane of the exposed surface and atoms move in the plane to compensate for the loss of the nearest neighbors. The reconstruction/relaxation energy can be calculated, but only by taking an un-relaxed slab with the exact same terminations on both sides of the slab and then computing the relaxation of that slab[50]

$$E_R = \frac{(E_S^I - E_S^R)}{N_S} \qquad 18$$

Where E_R is the energy associated with the relaxation or reconstruction. E^I_S is the Energy of the slab un-relaxed and E^R_S is the energy of the slab after relaxation. N_S is the number of atoms involved in that relaxation.

Slabs of Fe_2P-TaN terminated either with the (0001), (0002) or mixed surface were analyzed. The lattice constants used were the ones calculated in previous chapters. The (0001) slab had 88 atoms (40 Tantalums and 48 Nitrogens), the (0002) slab had 80 atoms (44 Ta and 36 N) and the mixed slab had 1:1 stoichiometry with 96 atoms. Using the 96 atom slab which had both (0001) and (0002) surfaces the vacuum layer was determined and expanded until the energy converged (< 0.3 meV/at) and was 11 Ang for all calculations. Results of the vacuum expansion are shown in Figure 19 and show

convergence of the slabs energy even at 7 Ang vacuum thickness. A thicker vacuum (11Ang) was selected to allow for the Adatom experiments to be run.

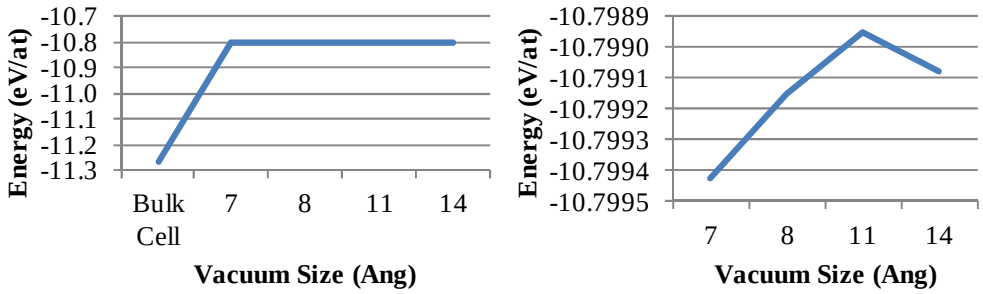

Figure 19. Graphs of the Vacuum expansion calculations of the Fe2P 96 atom cell, at different scales. Left side graph has the bulk cell energy/at for reference included in it.

To compare the surface energies between the two slabs, the following derivation is provided starting from an equation to calculate surface energy [74]

$$\sigma = \frac{1}{2A}(E_{Slab} - x_{Ta}\mu_{Ta} - x_N\mu_N + PV - TS) \quad (19)$$

Where A is the surface area of the slab, E_{Slab} is the energy of the slab. P, V, T and S are the pressure, volume, temperature and entropy, respectively. The number of Tantalums and Nitrogens in the slab are x_{Ta} and x_N, respectively. The chemical potentials (μ_{Ta} and μ_N) are for the chemical potentials of the elements in the compound. In *ab initio* calculations, T = 0 and PV ~ 0 and the equation is then

$$\sigma \cong \frac{1}{2A}(E_{Slab} - x_{Ta}\mu_{Ta} - x_N\mu_N) \quad (20)$$

The sum of the chemical potentials should be the chemical potential for the compound ($\mu_{Ta} + \mu_N = \mu_{TaN}$) and therefore the chemical potentials for the elements should be less.

$$\mu_Y \leq \mu_Y^{elem} \quad (21)$$

Where Y is either Ta or N. This is true or else the compound is not thermodynamically stable and would decompose into its constituents. For *ab initio* studies, the Gibb's free energy is the enthalpy (G = H – TS = H) as the calculations are done at T = 0 and the Enthalpy and Gibb's Free Energy are equivalent to the cohesive energy of a system. This gives the chemical potential for TaN.

$$\mu_{TaN} = \mu_{Ta} + \mu_N = \mu_{Ta}^{elem} + \mu_N^{elem} + \Delta H_{TaN} \quad (23)$$

Where ΔH_{TaN} is the Heat of Formation for TaN. Heat of Formation was calculated previously as calculated in Chapter 3 and was -1.19998 eV/at with a GGA-PBE PP, planewave cutoff of 520 eV, Kspace of 15x15x13 and gamma centered. In this case, Nitrogen is assumed to be in the N_2 gas state and Tantalum is in a BCC solid. Ta-BCC had a k-space of 9x9x9 with Monkhourst Pack centering and a_0 found to be 3.32 Ang with a planewave cut off was 520 eV using a GGA-PBE exchange correlation functional. The chemical potential was found to be -11.8324 eV/at. For the N_2 gas, planewave cutoff was set at 400 eV in a 30 Ang box and found to have a bond length of 1.11 Ang, and chemical potential was found to be -8.2996 eV/at.

By placing equation 6.6 into equation 6.4, a relationship between surface energy and chemical potential can be shown.

$$\sigma \cong \frac{1}{2A}(E_{Slab} - x_{Ta}\mu_{TaN} + (x_{Ta} - x_N)\mu_N) \quad (24)$$

Using this equation, it is possible to understand the relative surface energies of various planes based off this equation at 0 K and in a vacuum. Figure 20 shows the relative stability with varied chemical potential of Tantalum. It suggests that the (0001) surface is

most stable which is in agreement with single chemical potential point calculation that assumes the chemical potentials in the solid are the same as the chemical potentials of the individual atoms (i.e. decomposition/formation point). The Surface energy of the (0001) surface is always less than (0002) surface. It should be made clear that this is a relative measure of surface stability and conclusions about absolute surface stability are not complete.

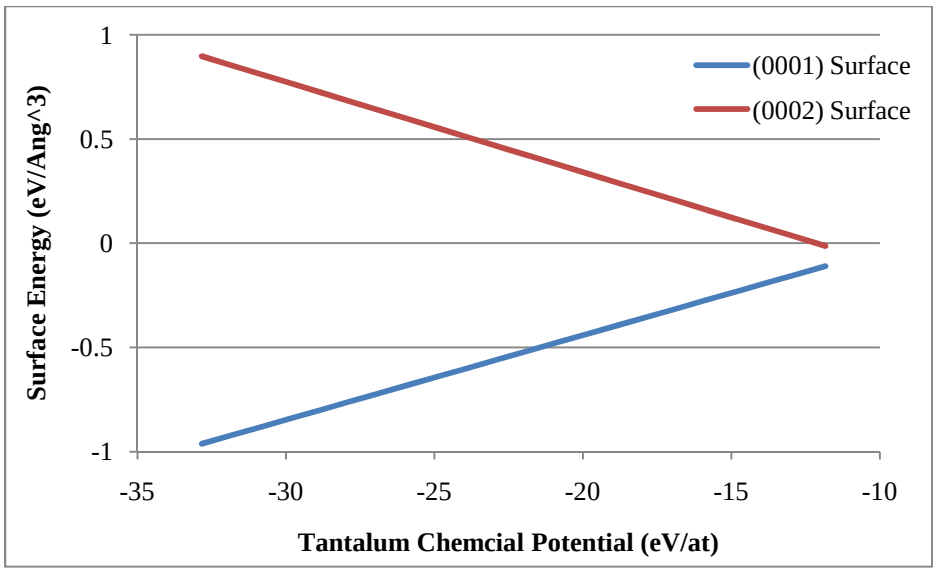

Figure 20. Surface Energy of the Fe_2P-TaN with (0001) and (0002) surfaces. The Tantalum chemical potential is varied as described.

To understand how the surface energy changes with increasing temperature and nitrogen gas pressure, the chemical potential for nitrogen can be written as[27, 74]

$$\mu_N = \mu^O_{N2,gas} + kTlnP_{N2} \qquad 25$$

Where k is Boltzmann's constant ($8.62x10^{-5}$ eV/K), T is temperature in Kelvin. P_{N2} is the partial pressure of the nitrogen. Combining equation 5 and 6 gives a means to calculate

the stability of the surfaces with increasing partial pressure of nitrogen and with increasing temperature. The equation is only valid if, Ta in TaN is thermodynamically favored ($\mu_{Ta} < \mu^{O}_{Ta,\ Bulk}$) and Nitrogen is more stable in the TaN ($\mu_{N} < \mu^{O}_{N2,\ gas}$). The final relation can be found by placing equation 24 and 25 into a single equation

$$\sigma \cong \frac{1}{2A}(E_{Slab} - x_{Ta}\mu_{TaN} + (x_{Ta} - x_N)(\mu^{O}_{N2,gas} + kTlnP_{N2})) \quad 26$$

A range of validity can be established for the calculation and by combining equations 23 and 25; the range can be shown to be

$$\frac{\Delta H^{O}_{TaN}}{kT} < lnP_{N2} < 0 \quad 27$$

The calculation will not be valid up to the triple point of the phase diagram depending on the partial pressure of nitrogen, but provides insight as to the stability region.

The surface energy of the (0001) and (0002) systems is shown in Table 15. The (0002) surface has a positive energy and therefore is unstable. The (0001) is lower in surface energy than the (0002) and therefore more stable. It should be noted that this technique is a relative technique and not intended to be used as an absolute measure of surface stability. Table 16 shows the Slab dimensional information. The (0001) surface shows an increase in the overall volume of the supercell after relaxation compared to the starting cell volume by 3.8% of the volume. The slab expands in the direction normal to the surface very little (-0.1% of the initial z), but the surface area for the slab increases by 4% compared to the starting surface. Looking at the atomic movements as shown in figure 6.4, the atoms move mostly normal to the surface, but do have a slight movement

away resulting in this increased surface. The top and bottom layers showed reduced lattice spacing for the (0001) to (0002) planes with the center 3 plans moving none. The (0001) terminated surface energy reduction upon relaxation is driven by inter layer relaxation.

Table 15. Surface energy calculated for Fe_2P.

	Area	N Atoms	Ta Atoms	Surface Energy
Units	Ang^2	#	#	eV/Ang^2
0001	98.5551	48	40	-0.159
0002	92.2953	36	44	0.039

The (0002) surface shows an overall decrease in the volume of the cell. The z axis increases by 2% and the area reduces by 2.7% compared to the initial cell size. The net result of this compression in one direction and expansion in the other is only a 0.7% reduction in the volume of the cell. The overall cell movement as shown in Figure 21 suggests the cell is compressing as all atomic movement is towards the z axis. There is minimal change shown in any of the inter-atomic distances between the (0001) and (0002) lattice plans. The (0002) cell suggests a compression in the cell and thus the energy reduction is associated with the slab itself reducing in energy as seen in Figure 22. This would suggest the system has a higher energy for the surface than reported. The 96 atom slab shows very little change in volume with the z axis compressing by 0.1% and the area increasing by 0.8%. The total cell volume only increases by 0.7%. The cell compresses in z by 0.1% and expanses in surface area by 0.8%. Figure 23 shows the system has very little atomic movement outside of the top 0002 and 0001 surfaces. The majority of the movement is in the direction of the surface and results in a reduction in the top lattice distances between in the (0001) and (0002). The mixed slab has a reduction in the interlayer space on for the (0001) surface and also shows the (0001)

surface re-arranged. This could support the fact that the (0001) is much more dynamic and capable of reducing its energy compared to the (0002).

Table 16. Slab information for the Fe_2P surface calculations.

	Starting Cell Vectors			Ending Cell Vectors			Cell Vol (Ang^3)	
Slab	X	Y	Z	X	Y	Z	Starting	Ending
Mixed	10.47	10.47	11.70	10.51	10.51	11.69	1118.00	1110.51
(0001)	10.47	10.47	10.24	10.67	10.67	10.23	1008.48	971.70
(0002)	10.47	10.47	10.24	10.32	10.32	10.45	964.60	971.70

Using the above derived equation for surface energies, further analysis was done to understand if there could be an inversion of the lowest energy surface upon changes in the temperature or upon introduction of a nitrogen atmosphere. The results of the analysis are shown in figure 24 and 25. As can be seen, there is no change in the fact that the (0001) is more stable than the (0002) surface. In addition, the (0002) surface only has a negative value at very high Temperature (1000K). Based on these results, the (0001) surface is used for all further Adatom calculations for both the Fe_2P phase and the CoSn phase.

Methods of Ag Adatoms on TaN

The absorption Enthalpy for silver on the surfaces of (0001) TaN-Fe_2P and TaN-CoSn is calculated with a GGA-PBE exchange correlation functional and a projector augmented wave (PAW) Pseudopotentials as previously described in Chapter 3. The planewave cutoff was 520 eV and the K space was 5x5x1 using a gamma centered K-space. The system relaxation was done by VASP's quasi-Newton algorithm for at least 4 ionic steps and convergence to 20 meV/at for ionic steps and electronic convergence to < 1 meV/at.

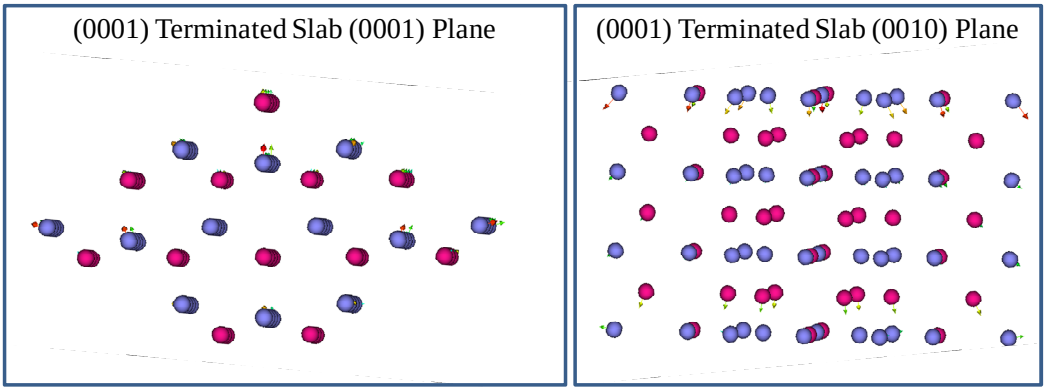

Figure 21. Atomic Movement of the (0001) terminated Fe_2P slab. Tantalum ( ) and Nitrogen ( )are shown.

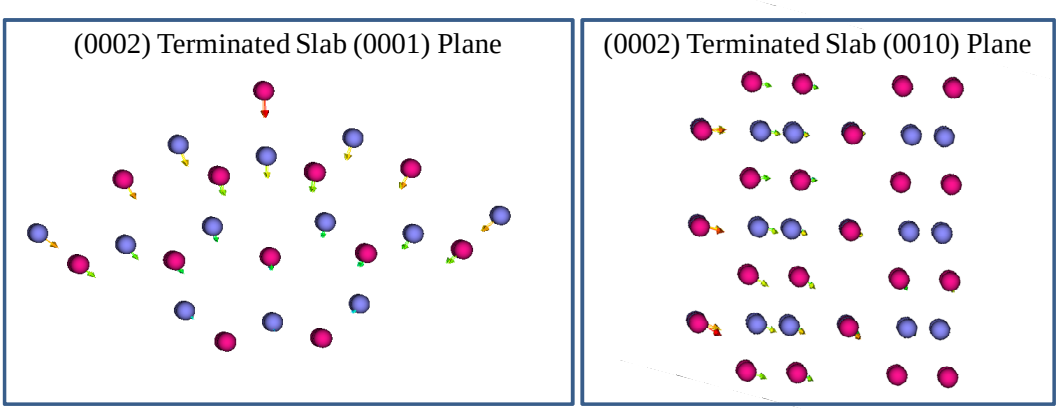

Figure 22. Atomic Movement of the (0002) terminated Fe_2P slab. Tantalum ( ) and Nitrogen ( ) are shown.

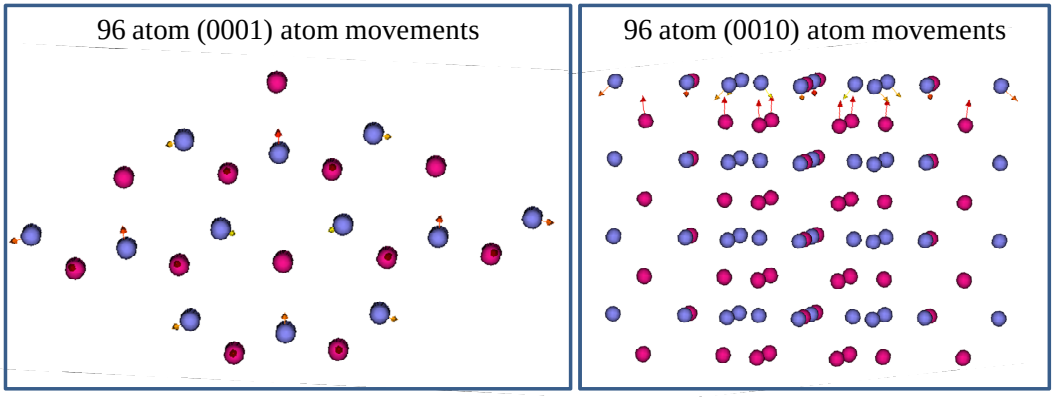

Figure 23. Atomic Movement of the mixed surface Fe2P slab. Tantalum ( ) and Nitrogen ( )are shown.

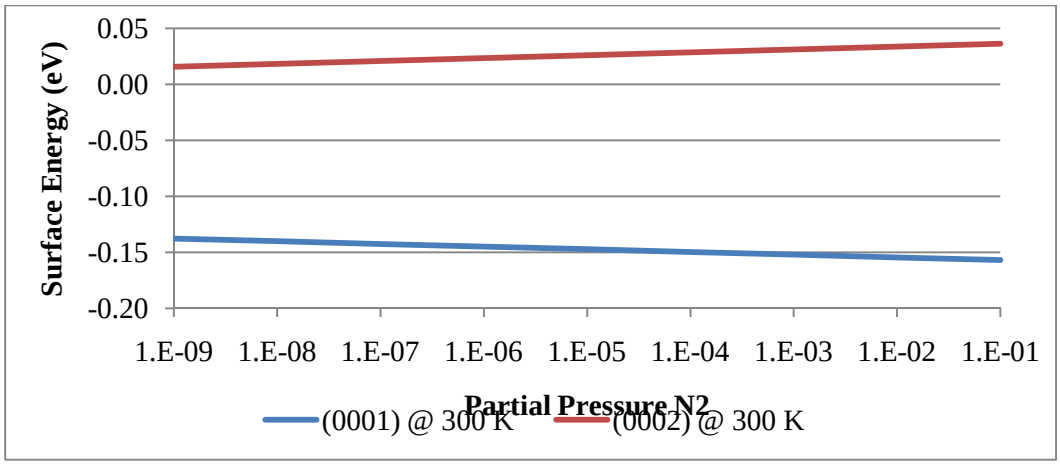

Figure 24. Surface energy calculation for the Fe2P-TaN at 300K

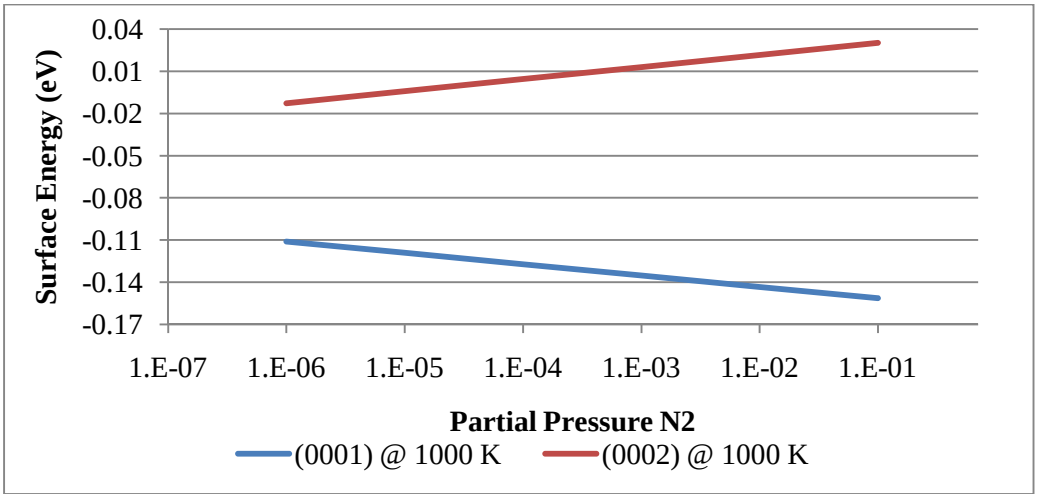

Figure 25. Surface energy calculation for the Fe_2P-TaN at 1000K

Slabs of CoSn and Fe_2P phases were analyzed to determine Adatom Absorption energies of silver on the lowest surface energy surface. The Ag Adatom energy was determined by the following equation.

$$E_{Absorption} = E_{Slab+Ag} - E_{Slab} - nE_{Ag} \quad (28)$$

Where the $E_{Slab+Ag}$, E_{Slab}, n and E_{Ag} are the energies for the slab with Ag Adatom(s), the slab without the Ag Adatom, the number of Ag Adatom and the energy of a single Ag atom in the gas phase, respectively. The starting location of the Silver Adatom was set

away from the near surface atom(s) as determined by the radius calculated from the Ag bulk calculations.

The silver atom in the gas and solid phase was calculated with a GGA-PBE PAW and a planewave cutoff of 450 eV. For the solid, K space was 17x17x17 and Monkhourst Pack centered. Solid phase was assumed to be FCC and the final lattice constant was 4.17 Ang. Heat of formation was -2.824 eV/at and -0.27157 eV/at for the solid and gas phases, respectively.

The 4 locations investigated for the CoSn phase are shown in Figure 6.9 and include the Hollow location above the (0002) Tantalum (Hollow A), the Hollow formed by the (0001) Nitrogens and Tantalum (Hollow B), Atop the Nitrogen and Atop the (0001) Tantalum. The CoSn phase system was a 216 base cell with the Silver Adatom added to the above listed locations.

For the Fe2P system, only the Hollow A and Hollow B sites were investigated, since the structure is similar to CoSn, and the Atop Nitrogen and Atop Tantalum sites were very unfavorable for CoSn.

For investigations of two silver adatoms on Fe2P, two geometries were considered, one with the Ag adatoms close together on Hollow-A sites, and one with them far apart on Hollow-A sites – see figure 27.

The sub-monolayer study had a 66 % ML of Ag on the Fe2P-TaN (0001) surface with the entire Hollow A locations filled on the slab. Work of adhesion was calculated from this by the following equation[75, 76]

$$W_{adh} = E_{AB} - E_{B,\ Strained} - E_A \qquad 28$$

Where W_{adh} is the work of adhesion, E_{AB} is the Enthalpy of the Slab of A and B, $E_{B,\ Strained}$ is the strained slab of B (in this case Silver) and E_A is the slab of A (in this case Fe_2P-TaN).

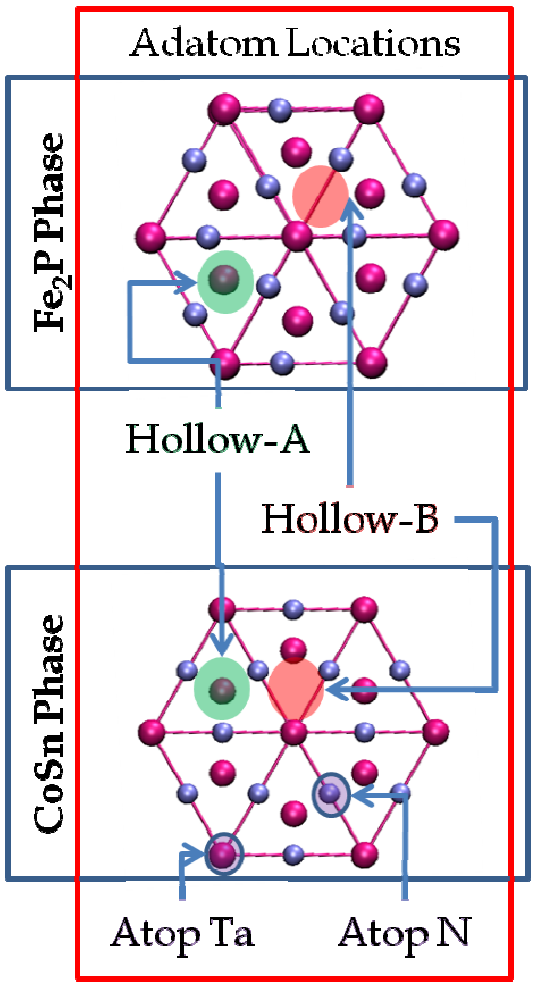

Figure 26. Location of Adatoms for both Fe_2P and CoSn phases.

Ag Adatom on CoSn-TaN

The results of the CoSn Adatom calculations are tabulated in Table 17 and atomic movements are shown in Figure 28. The largest absorption energy for the CoSn phase was for the Hollow-A site and resulted in the Ag Adatom being only 1.8Ang away from the (0001) surface. The (0002) Tantalum below the Ag atom moved towards the Ag. The second lowest energy is the Hollow B site and is close in absorption energy of the Atop Ta atom. By far, the Atop N is smallest in absorption energy.

The Hollow-A site is preferred because the Silver ends up being surrounded by Nitrogens in the Hollow A site and fits into a position that a tantalum would fit into on

the next layer above the surface. Hollow B could be viewed as an interstitial like site and as Tantalum Nitride have very tight bonding occurring between the Tantalum and the Nitrogen, interstitials the size of a Silver Ion would cause stress in such a lattice and would not be a favorable position. The Atop Atom locations would basically be the minimal amount of bonding possible in the system. It should be noted this is consistent with results of other Nitrides and Carbides as noted in Chapter 2.

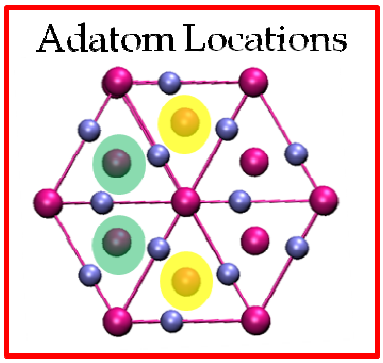

Figure 27. Location of proximity effects of adatoms with Hollow A locations populated with Ag adatoms. Green is the placement of the close Ag adatoms and yellow is the far distant placement.

The distance to the (0001) surface is the same for the Hollow-B, Atop N and Atop Ta Adatom and is consistent with the absorption energies being lower when compared to the Hollow-A and is a result of the reduced bonding for the Ag adatoms to the 3 sites The Hollow-B and Atop Ta both showed movement of the (0002) Ta atom below and closest to the Adatom compared to the Atop N and Hollow Adatom locations which showed no movement of the lower Ta (0002) atom. The Atop N did show some movement of the Nitrogen directly below the Ag Adatom and the Hollow-B site showed the Tantalum in the (0001) moving inward and away from the Ag Adatom. These movements suggest the Silver is attempting to locate itself similar to where a Tantalum would be if another layer of (0002) was added to the TaN-CoSn phase.

Table 17. Adatom surface energies and atomic movements calculated for the (0001) CoSn-TaN surface.

Adatom Location	Ag Absorption Energy (eV/at)	Ag Distance to 0001 (Ang)	NN Movement	NN Movement distance (Ang)	Direction moved
Atop N	-0.98	2.7	N	0.1	Towards Ag
Atop Ta	-1.15	2.7	Ta (0001)	0.1	Away from Ag
Hollow B	-1.16	2.7	Ta (0001)	0.1	Away from Ag
Hollow-A	-1.72	1.8	Ta (0002)	0.14	Towards Ag

Ag Adatom on Fe_2P-TaN

The 2 hollows of the Fe_2P-TaN (0001) surface were analyzed and it was found the Hollow-A location showed greater absorption energy when compared to the Hollow-B site with the Absorption Energies in Table 18. The Hollow A location has a larger number of Nitrogens for the Silver to bond to and is in the same location that another (0002) Tantalum would occur, thus allowing the Nitrogens to reduce the amount of broken bonds they have in the structure and approach the 5 fold coordination of the nitrogens in the bulk. The hollow B location is actually not a repeat site from the (0002) layer in addition to placing the Tantalum and Silvers in close proximity and resulting in them sharing the same Nitrogen's. The single Adatom study shows that the Hollow A location appears to be the lowest of two studied. There are other places such as bridge sites and Atop sites that the Adatom could be placed. The Hollow A site should be more stable when compared to these other sites. The reason is the other sites result in the surface atoms deviating further from the bulk state and due to the fact that the Adatom has less to interact with for bonding. The Hollow-A site is considered to be the most stable absorption site on the (0001) TaN-Fe_2P surface.

Next, 2 two-Adatom studies were done with one having adjacent Hollow A location (distance Ag to Ag is 3.01 Ang) and the other one having the Hollow A sites separated as far as possible in the supercell (distance is 6.02 Ang) as shown in Figure 27. This resulted in the Absorption energy being 1.160 and 1.159 eV/at for the close and far

Adatom results, respectively. The distances are provided in Table 18. The stability of the far and close absorption values suggest that additional Ag adatoms would fill all available Hollow A sites on the surface, forming a sub-monolayer of a FCC (111) plane with a small lattice mismatch of about 2%.

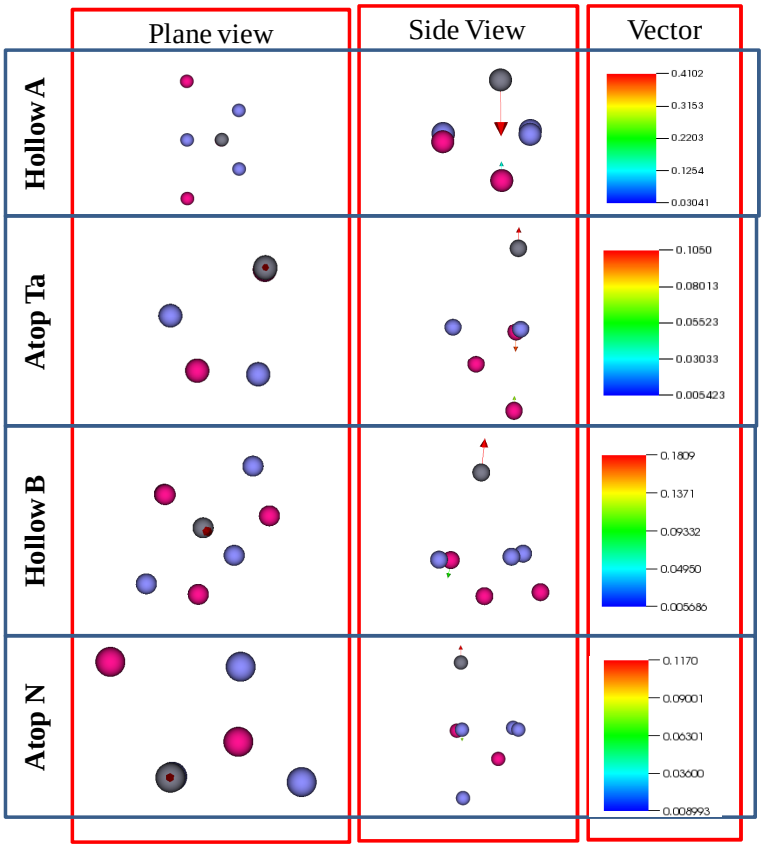

Figure 28. Adatom movements for the CoSn-TaN (0001) surface. Tantalum ( ), Silver ( ) and Nitrogen ( )are shown. Vector magnitudes are varied with legend provided.

Table 18. Enthalpies of Hollow Adatoms on Fe_2P-TaNstudies.

Hollow Location	Enthalpy of absorption (eV/at)	d_{Ag-N} (Ang)	d_{Ag-Ta} (Ang)
A	-1.335	2.22	2.77
Hollow B	-0.833	2.15; 2.26; 2.70	2.56
A, 2 Adatoms - close	-1.160	2.18	2.71
A, 2 Adatoms far	-1.159	2.18	2.70

Several studies were done on smaller cells to investigate the adhesion of Ag submonolayers (0.33 ML and 0.66 ML) and a 5 layer Ag slab to Fe2P-TaN. The smaller cell was a 24 atom TaN cell with same dimensions as the 216 cell used in the Adatom studies. All other parameters were the same between the 216 cell and the small 24 atom cell. The k points for the 24 atom cell showed convergence to< 1 meV/at for 5x5x1 k points. The smaller cell had 2 Hollow-A locations. The initial starting point for how far the silvers were placed was based on the adatom distances. For all calculations involving the TaN slab, only the ionic positions were allowed to relax with the cell shape and volume held constant. At least 8 ionic convergence steps were used for each of the studies and it was found that ionic convergence was < 1 meV/at for all calculations. For the work of adhesion calculation with the silver slab, the slab enthalpy was determined 2 different ways. First for the unrelaxed silver slab, it was electronically converged only with all ion positions held constant based off the full slab of TaN-Ag. For the relaxed silver slab, the ionic positions, cell shape and cell volume was allowed to relax completely. Results of the calculations are shown in table 19.

The Work of Adhesion is negative for all results and actually has the highest value for the unrelaxed 4-layer slab. This suggests that an interface between Silver and (0001) Fe_2P-TaN should be stable. In addition, the monolayer energies are slightly lower when compared to the slab values. This would cause an issue during creation of the interface as the bonding is not strong between the Silver and Tantalum Interface initially. *This drop in energy for the monolayer work of adhesion to when a thin slab of Tantalum nitride is formed can be explained by the fact that the bonding is changing between the Silver slab versus the ML structure vs the 4 Layer structure. This is supported by the*

fact that the distances between the silver and the nitrogen are increasing with the following order noted 1 Adatom<0.33 ML<0.66 ML< 4 layer slab.

Table 19: Work of Adhesion calculations for Silver on Tantalum Nitride

Silver Slab Structure	Work of Adhesion (J/m^2)	d_{Ag-N} (Ang)	d_{Ag-Ta} (Ang)
0.33 ML	-0.65	2.37	3.08
0.66 ML	-0.61	2.51	3.18
4 Layer - strained	-1.03	2.59	3.3
4 Layer - unstrained	-0.77	NA	NA

Summary

Calculation of the bond strength of a single Ag atom with a single Ta or N atom found that the Nitrogen-Silver bond energy was higher. This suggests that a Ag film would adhere more strongly to a Nitrogen rich surface than to a Tantalum rich surface.

The lowest energy surface was shown to be the (0001) for the Fe_2P-TaN surface as compared to the (0002) surface. The major difference between the two surfaces is the (0002) is Tantalum rich and has no Nitrogen terminations. The (0001) surface has a 3:1 ratio of Nitrogen to Tantalum. The (0001) was chosen as it would be enthalpically more stable. The (0001) surface was used for Adatom studies with Fe_2P-TaN and CoSn-TaN studies. For the CoSn-TaN (0001) surface, Silver adatoms were placed at 4 locations. It was found that the site of absorption would be a hollow site (Hollow A) which would result in the continuation of the crystal from the (0002) layer. The other sites were found to be less energcially stable. For the Fe_2P-TaN (0001) surface, Silver adatoms were placed on 2 hollow locations. The hollow site which continued the crystal structure (hollow A) was shown to be significantly lower in energy. Investigations of 2 Ag Adatom studies showed that the distance between the Ag adatoms did not significantly

affect their adsorption energy, which was slightly less than that of the single adatom. This suggests that silver deposited on a (0001) Fe2P-TaN surface should form initially by adatoms adhering to the Hollow A locations and continuing the crystal structure of the Fe2P-TaN. This results in the formation of a (111) FCC surface, slightly strained, with 1/3 of the first monolayer missing due to the presence of Ta adatoms in the (0001) plane. The work of adhesion was calculated from a 0.66 ML of Silver and resulted in a 0.61J/m^2 surface energy, which is modest.

The 2 atom and Adatom studies suggest that silver and TaN should form a stable interface. Upon calculation of the monolayers and slab, it is found that the silver has a modest work of adhesion on the Tantalum Nitride surface. This suggests that Fe2P-TaN/Ag maybe a viable candidate for interconnects. Further increase in the Ag slab thickness may not be stable. The slab will be epitaxial or result in Silver islands forming on the surface due to the lattice mismatch. An adhesion layer maybe still necessary for the Silver-TaN interconnect system.

Chapter 7

SUMMARY

Bulk Tantalum Nitride

The stability of three 1:1 stoichiometric compounds of Tantalum Nitride was investigated with three separate exchange correlation functionals (LDA, GGA-PBE, and GGA-PW91). For all exchange-correlation functionals, the order of stability of the crystal structures are Fe_2P > NaCl > CoSn at zero Kelvin. This demonstrates that the TaN-Fe_2P crystal structure is the ambient phase and should be used as such in future studies.

The bonding of the 3 systems was studied. It is shown that all three are metallic in nature, this is consistent with other *ab initio* studies. The NaCl bonding has the simplest structure where as the Fe_2P and CoSn phases are a little more complex. The Fe_2P system appears to have a small difference in how the two types of Tantalums bond to the Nitrogen with a slightly greater bonding associated with the Tantalum residing in the (0002) layer. The CoSn seems to have the Tantalum in the (0001) plane not significantly bonding with the (0002) Tantalum nor with the Nitrogen's in the system.

In addition, it was shown that the Fe_2P and also the CoSn phase showed fairly high vacancy formation energy. This would support a line compound as shown in the phase diagram. In contrast, the NaCl phase has a negative formation energy associated with Tantalum vacancy, suggesting it prefers a composition somewhat to the Ta rich side of the 1:1 stoichiometry, consistent with the phase diagram. Additional vacancies are also easily formed from 43at% to 50at% Ta suggesting that the NaCl phase will exist at a broad range of compositions, consistent with the phase diagram.

Surface Studies

The (0001) and (0002) surfaces were analyzed for their relative surface energies in the Fe_2P phase. It has been shown that the (0001) surface should be the lower surface energy system and that it could be easily maintained in a Nitrogen rich atmosphere. The (0001) surface was used for subsequent Adatom studies for both the CoSn and the Fe_2P systems.

The surface studies showed that the Hollow A location, which is where the (0002) surface continues for both the Fe_2P and CoSn, was the most enthalpically favorable location for the Silver Adatom. In addition for the Fe_2P phase, it was shown that 2 adatoms in either adjacent or farther way locations would have equivalent adsorption energies, slightly less per atom than for the single adatom. Finally, the work of adhesion for silver monolayer and four layer slabs appears to have modest to low adhesion to the TaN surface studied. The bonding appears to be ionic in nature based on the charge density plots. The monolayer has lower adhesion than when compared to the slab and maybe due to the second Ag layer interacting with the Tantalums on the (0001) at the interface.

Concluding remarks on Interconnect Directions

This study focused on the thermodynamics and adhesion of the TaN/Ag interconnect system. It suggests that Ag Adatoms binds strongly to TaN, but an adhesion layer such as Ta may still be needed as the Silver Monolayer binds weakly to the Tantalum Nitride. If one could eliminates the Tantalum adhesion layer, it would reduce the interconnect cross section, and greatly simplifies the interconnect processing. Further study is needed to understand subtleties of the integration to determine if the switch to TaN/Ag interconnects system would be worthwhile.

Potential Future Research

For the Tantalum Nitride system, the stability of the various Polymorphs of TaN should be studied further and in more depth. Experimentally, an assessment of the crystal structures should be done with Neutron scattering to validate the hypothesized results. For the TaN-Ag system, additional studies on the electrical properties and adhesion characteristics of low resistive metals such as silver, gold or copper should be done to understand if there are alternate barrier layers which may eliminate the need for adhesion layers or to propose alternate interconnect systems. In addition, the electrical properties of the interconnect should be studied to understand in an ideal case if the Tantalum Nitride-Silver interconnect has better conduction than currently shown by experiments.

Further studies could help understand how to increase the work of adhesion between Silver and Fe_2P-TaN by alloying the metal, inducing surface defects in the TaN surface or both and adhesion layers for improving the binding of silver to Tantalum Nitride should be explored. In addition, studies should be run as to how various Adatom elements, such as Ruthenium, may interact with the interface to allow direct electroplating of Silver to the Interconnect. Larger slabs of TaN-Silver should be run to understand how this system behaves with additional layers.

REFERENCES

1. Okamoto H. N-Ta (nitrogen-tantalum). Journal of Phase Equilibria and Diffusion 2008; 29(3):291

2. Interconnect. In: International technology roadmap for semiconductors. ; 2009.

3. Bohr MT. Interconnect scaling - the real limiter to high performance ULSI. Solid State Technol 1996 SEP; 39(9):105

4. Badenes G, Deferm L. Integration challenges in sub-0.25 mu m CMOS-based technologies. Microelectron J 2000; 31(11-12):861-71.

5. Travaly Y, Bamal M, Carbonell L, Iacopi F, Stucchi M, Van Hove M, Beyer GP. A novel approach to resistivity and interconnect modeling. Microelectronic Engineering 2006;83(11-12):2417-21.

6. Li W, Tan CM, Hou Y. Dynamic simulation of electromigration in polycrystalline interconnect thin film using combined monte carlo algorithm and finite element modeling. J Appl Phys 2007;101(10).

7. Li BZ, Sullivan TD, Lee TC, Badami D. Reliability challenges for copper interconnects. Microelectronics Reliability 2004;44(3):365-80.

8. Lane MW, Liniger EG, Lloyd JR. Relationship between interfacial adhesion and electromigration in cu metallization. J Appl Phys 2003;93(3):1417-21.

9. Interconnect. In: International technology roadmap for semiconductors. ; 2007.

10. Wang SQ, Ye HQ. Theoretical studies of solid-solid interfaces. Current Opinion in Solid State & Materials Science 2006;10:26-32.

11. Siegel DJ, Hector LG, Adams JB. Ab initio study of al-ceramic interfacial adhesion. Physical Review B 2003;67(9).

12. Kim H. Atomic layer deposition of metal and nitride thin films: Current research efforts and applications for semiconductor device processing. Journal of Vacuum Science & Technology B 2003 NOV-DEC;21(6):2231-61.

13. Lundqvist BI, Bogicevic A, Carling K, Dudiy SV, Gao S, Hartford J, Hyldgaard P, Jacobson N, Langreth DC, Lorente N, et al. Density-functional bridge between surfaces and interfaces. Surf Sci 2001;493(1-3):253-70.

14. Ooi N, Hector LG, Jr., Adams JB, Stanzione D, Jr. First principles study of the aluminum-cubic boron nitride interface. J Adhesion 2006 Aug;82(8):779-803.

15. Siegel D, Hector L, Adams J. First-principles study of metal-carbide/nitride adhesion: Al/VC vs. Al/VN. Acta Materialia 2002 FEB 8;50(3):619-31.

16. Siegel D, Hector L, Adams J. Ab initio study of al-ceramic interfacial adhesion. Physical Review B 2003 MAR 1;67(9):092105.

17. Pletea M, Wendrock H, Kaltofen R, Schmidt OG, Koch R. Stress evolution during and after sputter deposition of thin cu-al alloy films. Journal of Physics-Condensed Matter 2008;20(25).

18. Ding PJ, Lanford WA, Hymes S, Murarka SP. Effects of the addition of small amounts of al to copper - corrosion, resistivity, adhesion, morphology, and diffusion. J Appl Phys 1994;75(7):3627-31.

19. Strehle S, Menzel S, Bartha JW, Wetzig K. Electroplating of cu(ag) thin films for interconnect applications. Microelectronic Engineering 2010 2;87(2):180-6.

20. CRC handbook of chemistry and physics. 1978.

21. Alford TL, Misra E, Bhagat SK, Mayer JW. Influence of joule heating during electromigration evaluation of silver lines. Thin Solid Films 2009 JAN 1;517(5):1833-6.

22. Alford TL, Misra E, Bhagat SK, Mayer JW. Influence of joule heating during electromigration evaluation of silver lines. Thin Solid Films 2009 JAN 1;517(5):1833-6.

23. Bhagat SK, Theodore ND, Alford TL. Thermal stability of tungsten-titanium diffusion barriers for silver metallization. Thin Solid Films 2008 SEP 1;516(21):7451-7.

24. Baunemann A. Precursor chemistry of tantalum and niobium nitride for MOCVD and ALD applications. zur Erlangung der Doktorwürde der Fakultät für Chemie der Ruhr-Universität Bochum; 2006.

25. Cao CL, Hou ZF, Yuan G. First-principles study of the structural stability and electronic structures of TaN. Physica Status Solidi B-Basic Solid State Physics 2008;245(8):1580-5.

26. Kim TE, Han S, Son WJ, Cho E, Ahn HS, Shin S. Phase stability and electronic structures of stoichiometric tantalum mononitrides. Computational Materials Science 2008;44(2):577-80.

27. Stampfl C, Freeman AJ. Stable and metastable structures of the multiphase tantalum nitride system. Physical Review B 2005 JAN;71(2):024111.

28. Zhao EJ, Wu ZJ. Electronic and mechanical properties of 5d transition metal mononitrides via first principles. Journal of Solid State Chemistry 2008;181(10):2814-27.

29. Violet P, Blanquet E, Le Bacq O. Density functional study of the stability and electronic properties of TaxNy compounds used as copper diffusion barriers. Microelectronic Engineering 2006;83:2077-81.

30. Stampfl C, Freeman AJ. Metallic to insulating nature of TaNx: Role of ta and N vacancies. Physical Review B 2003 FEB 1;67(6):064108.

31. Zhou J, Chen H, Li Y. Diffusion barrier performance of nanoscale TaNx thin-film. Transactions of Nonferrous Metals Society of China 2007 8;17(4):733-8.

32. Zhao Y, Lu G. First-principles simulations of copper diffusion in tantalum and tantalum nitride. Physical Review B 2009;79(21).

33. Zhao EJ, Hong B, Meng J, Wu ZJ. First principles investigation on the ultra-incompressible and hard TaN. Journal of Computational Chemistry 2009;30(14):2358-63.

34. Iwamoto N, Truong N, Lee E. New metal layers for integrated circuit manufacture: Experimental and modeling studies. Thin Solid Films 2004;469:431-7.

35. CHRISTENSEN A, LEBECH B. Reinvestigation of structure of epsilon-tantalum nitride. Acta Crystallographica Section B-Structural Science 1978;34(JAN):261-3.

36. Ren F, Wang Y. Pressure-induced phase transition of tantalum mononitride. Thin Solid Films 2011 MAR 31;519(11):3954-8.

37. Capelle K. A bird's-eye view of density-functional theory. Brazilian Journal of Physics 2006;36(4A):1318-43.

38. Spencer ND, Moore JH. Encyclopedia of chemical physics and physical chemistry. Bristol ; Philadelphia: Institute of Physics Pub; 2001. 3 v.

39. Mattsson AE, Schultz PA, Desjarlais MP, Mattsson TR, Leung K. Designing meaningful density functional theory calculations in materials science - a primer. Model Simul Mater Sci Eng 2005;13(1):R1-R31.

40. Hummel RE. Electronic properties of materials. 2nd ed. Berlin ; New York: Springer-Verlag; 1992. xv; ill. ; 24 cm.

41. Reuter K, Stampfl C, Scheffler M. Ab initio atomistic thermodynamics and statistical mechanics of surface properties and functions. Handbook of materials modeling. 2005.

42. Ellis DE, Warschkow O. Evolution of classical/quantum methodologies: Applications to oxide surfaces and interfaces. Coord Chem Rev 2003;238:31-53.

43. Hafner J. Ab-initio simulations of materials using VASP: Density-functional theory and beyond. Journal of Computational Chemistry 2008;29(13):2044-78.

44. Pacchioni G. Ab initio theory of point defects in oxide materials: Structure, properties, chemical reactivity. Solid State Sciences 2000;2(2):161-79.

45. Fiolhais C, Nogueira F, Marques M. A primer in density functional theory. Berlin ; New York: Springer; 2003. xii; ill. ; 24 cm.

46. Mishin Y, Asta M, Li J. Atomistic modeling of interfaces and their impact on microstructure and properties. Acta Materialia 2010 2;58(4):1117-51.

47. Kresse G, Marsman M, Furthmuller J. VASP the guide. ; 2009.

48. Jahnatek M, Krajci M, Hafner J. Interatomic bonding, elastic properties, and ideal strength of transition metal aluminides: A case study for al-3(V,ti). Physical Review B 2005;71(2).

49. Siegel DJ. First-principles study of metal-ceramic interfaces. University of Illinois at Urbana-Champaign; 2001.

50. Ooi N. Theoretical study of aluminum ceramic interfaces. Arizona State University; 2005.

51. Hafner J. Materials simulations using VASP - a quantum perspective to materials science. Comput Phys Commun 2007;177(1-2):6-13
.
52. Blochl PE. Phys Rev B 1994(50):17953.

53. Kresse G, Joubert J. From ultrasoft pseudopotentials to the projector augmented wave method. Phys Rev B 1999;59:1758.

54. Perdew JP, Burke K, Wang Y. Generalized gradient approximation for the exchange-correlation hole of a many-electron system. Physical Review B 1996 DEC 15;54(23):16533-9.

55. Perdew J, Chevary J, Vosko S, Jackson K, Pederson M, Singh D, Fiolhais C. Atoms, molecules, solids, and surfaces - applications of the generalized gradient approximation for exchange and correlation (vol 46, pg 6671, 1992). Physical Review B 1993 AUG 15;48(7):4978.

56. Perdew J, Burke K, Ernzerhof M. Generalized gradient approximation made simple (vol 77, pg 3865, 1996). Phys Rev Lett 1997 FEB 17;78(7):1396.

57. Perdew J, Burke K, Ernzerhof M. Generalized gradient approximation made simple. Phys Rev Lett 1996 OCT 28;77(18):3865-8.

58. Perdew J, Chevary J, Vosko S, Jackson K, Pederson M, Singh D, Fiolhais C. Atoms, molecules, solids, and surfaces - applications of the generalized gradient approximation for exchange and correlation. Physical Review B 1992 SEP 15;46(11):6671-87.

59. Perdew J, Zungar A. Self-interaction correction to density-functional approximations for many-electron systems. Physical Review B 1981;23(10):5048-79.

60. Mavromaras A, Rigby D, Wolf W, Christensen M, Halls M, Freeman C, Saxe P, Wimmer E. Computational materials engineering: Capabilities of atomic-scale prediction of mechanical, thermal, and electrical properties of microelectronic

materials. 11th. Int. Conf. on Thermal, Mechanical and Multiphysics Simulation and Experiments in Micro-Electronics and Micro-Systems, EuroSimE 2010 2010.

61. Humphrey W, Dalke A, Schulten K,. VMD - visual molecular dynamics. Journal of Molecular Graphics 1996;14:33.

62. VisIT Visualization Tool [Internet]; c2012 [cited 2012 3/18]. Available from: https://wci.llnl.gov/codes/visit/home.html.

63. Siegel D, Hector L, Adams J. Ab initio study of al-ceramic interfacial adhesion. Physical Review B 2003 MAR 1;67(9):092105.

64. Henkelman G, Arnaldsson A, Jonsson H. A fast and robust algorithm for bader decomposition of charge density. Computational Materials Science 2006 JUN;36(3):354-60.

65. Tang W, Sanville E, Henkelman G. A grid-based bader analysis algorithm without lattice bias. Journal of Physics-Condensed Matter 2009 FEB 25;21(8):084204.

66. Murnaghan FD. The compressibility of media under extreme pressures. Proc Natl Acad Sci U S A 1944;30:244-7.

67. Wang H, Hon H. Temperature dependence of ceramic hardness. Ceramics International 1999;25:267.

68. Chuang W, Luger T, Fettig R, Ghodssi R. Mechanical property characterization of LPCVD silicon nitride thin films at cryogenic temperatures. J Microelectromech Syst 2004 OCT;13(5):870-9.

69. Patil SKR, Mangale NS, Khare SV, Marsillac S. Super hard cubic phases of period VI transition metal nitrides: First principles investigation. Thin Solid Films 2008 11/28;517(2):824-7.

70. Sahnoun M, Daul C, Driz M, Parlebas JC, Demangeat C. FP-LAPW investigation of electronic structure of TaN and TaC compounds. Computational Materials Science 2005;33(1-3):175-83.

71. Portnoi, Mukaseev, Gribkov, Levinskii, Prokof'ev. Modulus of elasticity of some refractory compounds. 1967:185.

72. Mah G. Heats of formation of niobium nitride, tantalum nitride and zirconium nitride from combustion calorimetry. 1956;78:3261.

73. DeHoff RT. Thermodynamics in materials science. McGraw-Hill; 1993.

74. Jiang Y. Gas-solid interface reactons of metals and metal oxides. Arizona State University; 2005.

75. Hashibon A, Elsasser C, Ruhle M. Structure at abrupt copper-alumina interfaces: An ab initio study. Acta Materialia 2005;53(20):5323-32.

76. Finnis MW. The theory of metal–ceramic interfaces. Journal of Physics-Condensed Matter 1996;8:5811.

APPENDIX A

POSCAR FOR HEXAGONAL STRUCTURES

Fe_2P-TaN Base cell

5.49031026300000

0.7900851066372291 -0.4783611630944735 0.2270683073954599

0.0000000000000000 0.9567223261889469 0.0000000000000000

-0.1411284651367380 0.0000000000000000 0.5123937291282264

3 3

Direct

0.0000000000000000 0.0018710991651716 0.0000000000000000

0.3340839407777310 0.6665966571857496 0.4984335890447085

0.6659160592222690 0.3325127164080257 0.5015664109552915

0.3916426385735434 0.9984020752827405 0.0005600333088580

0.0000000000000000 0.3938580152491156 0.0000000000000000

0.6083573614264566 0.6067594367091971 0.9994399666911420

CoSn-TaN Base Cell

5.27 ! Run 3

0.500000 -0.866025 0.000000

0.500000 0.866025 0.000000

0.000000 0.000000 0.555977

3 3

Direct

0.00000000 0.00000000 0.00000000

0.33333333 0.66666667 0.50000000

0.66666667 0.33333333 0.50000000

0.50000000 0.00000000 0.00000000

0.00000000 0.50000000 0.00000000

0.50000000 0.50000000 0.00000000

APPENDIX B

COPYWRITE PERMISSION

SPRINGER LICENSE
TERMS AND CONDITIONS

Jan 22, 2012

This is a License Agreement between Michael G Grumski ("You") and Springer ("Springer") provided by Copyright Clearance Center ("CCC"). The license consists of your order details, the terms and conditions provided by Springer, and the payment terms and conditions.

All payments must be made in full to CCC. For payment instructions, please see information listed at the bottom of this form.

License Number	2834470566234
License date	Jan 22, 2012
Licensed content publisher	Springer
Licensed content publication	Journal of Phase Equilibria (and diffusion)
Licensed content title	N-Ta (Nitrogen-Tantalum)
Licensed content author	H. Okamoto
Licensed content date	Jan 1, 2008
Volume number	29
Issue number	3
Type of Use	Thesis/Dissertation
Portion	Figures
Author of this Springer article	No
Order reference number	
Title of your thesis / dissertation	Ab initio Study of Mechanics and Thermodynamics of the TaN and Ag Adatoms
Expected completion date	May 2012
Estimated size(pages)	120
Total	0.00 USD
Terms and Conditions	

Introduction
The publisher for this copyrighted material is Springer Science + Business Media. By clicking "accept" in connection with completing this licensing transaction, you agree that the following terms and conditions apply to this transaction (along with the Billing and Payment terms and conditions established by Copyright Clearance Center, Inc. ("CCC"), at the time that you opened your Rightslink account and that are available at any time at http://myaccount.copyright.com).

Limited License
With reference to your request to reprint in your thesis material on which Springer Science and Business Media control the copyright, permission is granted, free of charge, for the use indicated in your enquiry. Licenses are for one-time use only with a maximum distribution equal to the number that you identified in the licensing process.

This License includes use in an electronic form, provided it is password protected or on the university's intranet, destined to microfilming by UMI and University repository. For any other electronic use, please contact Springer at (permissions.dordrecht@springer.com or permissions.heidelberg@springer.com)

The material can only be used for the purpose of defending your thesis, and with a maximum of 100 extra copies in paper.

Although Springer holds copyright to the material and is entitled to negotiate on rights, this license is only valid, provided permission is also obtained from the (co) author (address is given with the article/chapter) and provided it concerns original material which does not carry references to other sources (if material in question appears with credit to another source, authorization from that source is required as well). Permission free of charge on this occasion does not prejudice any rights we might have to charge for reproduction of our copyrighted material in the future.

Altering/Modifying Material: Not Permitted
However figures and illustrations may be altered minimally to serve your work. Any other abbreviations, additions, deletions and/or any other alterations shall be made only with prior written authorization of the author(s) and/or Springer Science + Business Media. (Please contact Springer at permissions.dordrecht@springer.com or permissions.heidelberg@springer.com)

Reservation of Rights
Springer Science + Business Media reserves all rights not specifically granted in the combination of (i) the license details provided by you and accepted in the course of this licensing transaction, (ii) these terms and conditions and (iii) CCC's Billing and Payment terms and conditions.

Copyright Notice:
Please include the following copyright citation referencing the publication in which the material was originally published. Where wording is within brackets, please include verbatim.
"With kind permission from Springer Science+Business Media: <book/journal

title, chapter/article title, volume, year of publication, page, name(s) of author (s), figure number(s), and any original (first) copyright notice displayed with material>."

Warranties: Springer Science + Business Media makes no representations or warranties with respect to the licensed material.

Indemnity
You hereby indemnify and agree to hold harmless Springer Science + Business Media and CCC, and their respective officers, directors, employees and agents, from and against any and all claims arising out of your use of the licensed material other than as specifically authorized pursuant to this license.

No Transfer of License
This license is personal to you and may not be sublicensed, assigned, or transferred by you to any other person without Springer Science + Business Media's written permission.

No Amendment Except in Writing
This license may not be amended except in a writing signed by both parties (or, in the case of Springer Science + Business Media, by CCC on Springer Science + Business Media's behalf).

Objection to Contrary Terms
Springer Science + Business Media hereby objects to any terms contained in any purchase order, acknowledgment, check endorsement or other writing prepared by you, which terms are inconsistent with these terms and conditions or CCC's Billing and Payment terms and conditions. These terms and conditions, together with CCC's Billing and Payment terms and conditions (which are incorporated herein), comprise the entire agreement between you and Springer Science + Business Media (and CCC) concerning this licensing transaction. In the event of any conflict between your obligations established by these terms and conditions and those established by CCC's Billing and Payment terms and conditions, these terms and conditions shall control.

Jurisdiction
All disputes that may arise in connection with this present License, or the breach thereof, shall be settled exclusively by the country's law in which the work was originally published.

Other terms and conditions:

v1.2

If you would like to pay for this license now, please remit this license along with your

payment made payable to "COPYRIGHT CLEARANCE CENTER" otherwise you will be invoiced within 48 hours of the license date. Payment should be in the form of a check or money order referencing your account number and this invoice number RLNK500703807.
Once you receive your invoice for this order, you may pay your invoice by credit card. Please follow instructions provided at that time.

Make Payment To:
Copyright Clearance Center
Dept 001
P.O. Box 843006
Boston, MA 02284-3006

For suggestions or comments regarding this order, contact RightsLink Customer Support: customercare@copyright.com or +1-877-622-5543 (toll free in the US) or +1-978-646-2777.

Gratis licenses (referencing $0 in the Total field) are free. Please retain this printable license for your reference. No payment is required.

BIOGRAPHICAL SKETCH

Michael G. Grumski graduated from University of Florida for his Masters and Bachelors of Science in Material Science and Engineering in 2000. In 2000, he married Bonnie Allyson Davis and moved to Arizona to work at Intel. As of 2012, he is a Staff Engineering at Intel focused on advanced process and technology development for products projected for production in 10 to 15 years.